

# The orbital content of bars: The origin of “non-x1-tree”, bar-supporting orbits

P.A. Patsis,<sup>1,2\*</sup> E. Athanassoula,<sup>2</sup>

<sup>1</sup>Research Center for Astronomy, Academy of Athens, Soranou Efessiou 4, GR-115 27, Athens, Greece

<sup>2</sup>Aix Marseille Université, CNRS, CNES, LAM, Marseille 13, France

Accepted .....Received .....;in original form .....

## ABSTRACT

Recently, many orbital studies in barred galaxy potentials have revealed the existence of orbits which are *not* trapped around x1-tree orbits, but could be potentially appropriate building blocks for bars. These findings question the uniqueness of the x1 family as the standard paradigm of orbital motion in galactic bars. The main goal of this paper is to investigate the role that such orbits could play in shaping the morphology of bars. We trace the morphological patterns appearing in the face-on and edge-on views of the non-periodic orbits presented in these studies and we show that they are introduced in the system by second type (“*deuxième genre*”) bifurcations of x1. For this purpose, we use a typical 3D Ferrers bar model and follow the radial and vertical bifurcations of the x1 family considered as being *mul*-periodic, with *mul* = 2, 3, 5. The variation of the stability indices of x1 in the *mul* = 2, 3 cases give us also the 4- and 6-periodic orbits, respectively. We tabulate these orbits including all information necessary to assess their role as appropriate building blocks. We discuss their stability and their extent, as well as their size and morphological evolution, as a function of energy. We conclude that even the most important of the *mul*-periodic orbits presented in Tables 2 to 5 are less appropriate building blocks for bars than the families of the x1-tree at the same energy.

**Key words:** Galaxies: kinematics and dynamics – Galaxies: spiral – Galaxies: structure

## 1 INTRODUCTION

In general, studies of orbital structure have shown that the basic building blocks of 2D bars are elliptical-like, elongated along the bar, single-periodic orbits confined within the corotation resonance, which are called x1 or B (Contopoulos & Papayannopoulos 1980; Athanassoula et al. 1983; Contopoulos & Grosbøl 1989, etc.). Bars, however, are not 2D objects. They have a considerable extent vertically to the equatorial plane of the galaxy and a rather complex shape (for a review see sect. 3.3 of Athanassoula 2016, and references therein). Building blocks for such a 3D bar could be the families of the x1-tree<sup>1</sup> (Skokos et al. 2002a; Patsis et al. 2002b), with elliptical-like projections on the equatorial plane. Many recent papers, however, discuss new building blocks with quite different morphology. Typical examples of such orbits can be found in Abbot et al. (2017, hereafter AVSD), Chaves-Velasquez et al. (2017), Deibel et al. (2011), Gajda et al. (2016, hereafter GLA), Katsanikas et al. (2011b, hereafter KPP), Machado & Manos (2016), Patsis & Katsanikas (2014a,b, hereafter PKa and PKb, respectively), Portail et al. (2015, hereafter PWG), Valluri et al. (2016, hereafter VSAD),

Wang et al. (2016, hereafter WAM) and Wozniak & Michel-Dansac (2009, hereafter WM-D). In some cases the face-on view of these orbits is complicated, while their edge-on views are similar to the projections of the frown-smiles orbits that are considered to build the peanut (see e.g. Skokos et al. 2002a). The orbits depicted in the figures of the above mentioned studies are not periodic, but their approximate morphology indicates that they are pretty near a periodic one, or that they are to a large extent determined by the presence of a radial or vertical resonance. The existence of these orbits raises the question, of whether the paths followed by stars in galactic bars are finally different from the generally accepted elliptical-like orbits. Elliptical-like projections of periodic orbits on the equatorial plane of barred galaxy models, with their major axes aligned with the major axis of the bar, are secured by the presence of x1 and its simple-periodic 3D bifurcations, i.e. by the orbits of the x1-tree, at least away from the regions of radial n:1 resonances with n > 2. Higher multiplicity periodic orbits have in general more complicated shapes, but could, in principle, still offer an alternative, more complicated, backbone of bars. In the present paper we address this possibility in view of the new results found recently in the above cited papers.

The periodic orbits (hereafter p.o.) found in 3D rotating bars belong to families, which in principle exist in every 3D rotating potential in autonomous Hamiltonian systems. Such systems can

\* patsis@academyofathens.gr (PAP)

<sup>1</sup> The set of families belonging to the x1-tree, includes x1 and its simple-periodic 3D bifurcations at the vertical n:1 resonances.

be written, in Cartesian coordinates  $(x, y, z)$ , in the form:

$$H = \frac{1}{2}(p_x^2 + p_y^2 + p_z^2) + \Phi(x, y, z) - \Omega_p(xp_y - yp_x), \quad (1)$$

where  $p_x$ ,  $p_y$ , and  $p_z$  are the canonically conjugate momenta and  $\Omega_p$  the angular velocity of the system (pattern speed). The numerical value of the Hamiltonian,  $E_J$ , is the Jacobi constant and we will also refer to it throughout the paper as the “energy”. We want to underline that it is not the presence of a specific barred component that gives rise to these families. Examples of models without an explicit bar component, where the same families appear can be found in Patsis & Zachilas (1990), Patsis & Grosbøl (1996), Patsis et al. (2002a) and Chaves-Velasquez et al. (2019). The morphology of the p.o. is determined merely by the presence of the radial and vertical resonances (Skokos et al. 2002a). These resonances exist in any model of a rotating three-dimensional potential.

Periodic orbits determine the dynamics of a dynamical system, since they determine the topology of the phase space. Around any stable p.o. there are islands of stability, while the unstable p.o. introduce chaotic motion. The multiplicity  $mul$  of a periodic orbit plays a key role as it gives the number of intersections of the p.o. with the surface of section in one direction (usually the upwards intersections are considered). Consequently, a p.o. of multiplicity  $mul$ , called a  $mul$ -periodic orbit, will have  $mul$  intersections with the surface of section. We note that  $mul$  depends on the chosen surface of section. A typical example is the two-dimensional (2D) case of a x1 orbit with loops at its apocenters (see e.g. the orbit in figure 2e in Skokos et al. 2002a). Placing the bar major axis along the y-axis, and considering the  $y = 0$  surface as surface of section, it is 1-periodic, while if we consider the surface of section  $x = 0$ , it is 3-periodic. Hereafter, in our orbital studies we use  $y = 0$  as cross section.

Among all p.o., the simple p.o. of multiplicity 1, or 1-periodic, play a key role. If stable, they are found at the centers of large stability islands in the surfaces of section. In potentials, which have a sufficiently strong bar, these islands are surrounded by a system of smaller islands forming what is often referred to as an archipelago. We have chains of smaller islands in resonance zones around the main island, in which stable-unstable pairs of p.o. alternate (see e.g. Contopoulos 2004). These are p.o. of multiplicity  $mul$  with  $mul > 1$ , frequently encountered in the literature in the terminology of Poincaré, namely as type II (second type, “*deuxième genre*”) orbits (Poincaré 1899). An attempt to visualize the succession of invariant tori and the chaotic filaments that connect the unstable p.o. in the 4D space of section of 3D Hamiltonian systems has been presented in KPP.

Tracing the *deuxième genre* orbits is not always an easy task, especially if the dimension of the system is larger than two. The standard tool frequently used for finding the families of periodic orbits and their connection with other bifurcating families in 3D Hamiltonian models, is the “stability diagram”, which gives the linear stability of the members of a family of p.o. as a parameter, (e.g.  $E_J$ ), varies (Contopoulos & Magnenat 1985). For calculating the linear stability of the periodic orbits in such systems we proceeded as Broucke (1969) and Hadjidemetriou (1975). Definitions and details about the algorithm we followed can be found e.g. in Skokos et al. (2002a). Here we briefly mention that the variation of the stability with  $E_J$  is described by the variation of two stability indices,  $b_1$  and  $b_2$ , one of which refers to the stability of the orbits of a family subject to radial and the other to vertical perturbations. A p.o. is stable (S) if both  $b_i \in (-2, 2)$ , with  $i = 1, 2$ . If one of the two stability indices is  $|b_i| > 2$ , then the orbit is characterized as simple

unstable (U), while if both indices are  $|b_i| > 2$  it is double unstable (DU). Finally if all four eigenvalues of the monodromy matrix are complex numbers off the unit circle, the stability indices cannot be defined and the p.o. is called complex unstable ( $\Delta$ ). In the case of 1-periodic orbits, whenever we have intersections or tangencies of one of the  $b_i$  stability curves with the  $b = -2$  axis, new families are bifurcated from the parent one, having the same multiplicity. On the other hand, tangencies or intersections with the  $b = 2$  axis bring into the system new families with multiplicity double that of the parent one (Contopoulos 1986).

In general, the critical value of a stability index at which a bifurcating family of multiplicity  $mul$  is introduced in the system is given by

$$b = -2 \cos\left(2\pi \frac{1}{mul}\right). \quad (2)$$

Thus, a family of p.o. of multiplicity  $mul = 1$ , reaching the  $b = -2$  axis as  $E_J$  varies, will bifurcate another family again with  $mul = 1$ , while families with  $mul = 2$  will appear, according to Eq. 2, at intersections or tangencies of a stability curve with the  $b = 2$  axis. A stability diagram of a 1-periodic family gives us the information about the  $E_J$  value at which 1- and 2-periodic families will be introduced in the system. However, for tracing further families with  $mul = 3, 4, 5$  etc. in the same diagram, we have to plot, besides the  $b = -2$  and  $b = 2$  axes, also the axes  $b = 1, 0, -0.618\dots$  and so on respectively (see Appendix A in Skokos et al. 2002b, for details).

An alternative way for following  $mul$ -periodic bifurcations of an 1-periodic family is to consider it as being itself of multiplicity  $mul$ , by repeating it  $mul$  times. Then, the stability curves will indicate the birth energies of the bifurcating families of multiplicity  $mul$  at their intersections, or tangencies, with the  $b = -2$  axis, while new families with multiplicity  $2mul$  will be introduced in the system, whenever  $b = 2$ . Hereafter, if not otherwise indicated, when we refer to  $mul$ -periodic orbits, we mean that  $mul \geq 2$ .

The goal of this paper is to find the origin of the orbital morphologies encountered in relevant recent papers on orbital structure cited in the first part of this introduction. In this effort we have to have in mind two things: Firstly that the shape of an orbit is influenced by the resonance in which it is introduced in the system, but also by the energy along the characteristic<sup>2</sup> at which a particular representative of a family is found. As an example one can observe the morphological evolution of x1 along its characteristic in various models, like figure 11 in Contopoulos (1983), figure 3 in Athanassoula (1992), or figure 2 in Skokos et al. (2002a). Secondly, that moving along the characteristic of a 3D family, each projection of a p.o. will follow its own morphological evolution. On top of this, the face-on and edge-on projections of the (not necessarily periodic) orbits may display the fingerprints of different radial and vertical resonances in their morphologies, depending on the location of its initial conditions in phase space. A certain face-on structure may be combined with different edge-on ones and vice versa. Thus, when we look for a specific face-on or edge-on morphology, essentially we want to identify the energy at which this specific structure is introduced in the system.

In our study we consider also the possibility that chaotic orbits may support the bar, or part of it. The role of chaotic orbits in supporting a bar has been investigated in several studies of 2D and 3D models (see e.g. Athanassoula et al. 1983; Patsis et al. 2010; Manos

<sup>2</sup> The characteristic of a family of p.o. is a curve that gives one (or more) initial condition of its members as a function of a parameter, usually  $E_J$ .

& Athanassoula 2011; Machado & Manos 2016, WAM). Note that PKa found that chaotic orbits close to the transition points from stability to complex instability (Contopoulos & Magennat 1985) may contribute in the reinforcement of features like the X's in edge-on views of the bars. In addition sticky chaotic orbits (Contopoulos & Harsoula 2008, see also figure 8 and corresponding text in Athanassoula et al. 1983) at the vertical 2:1 resonance (vILR) region (PKa, PKb), as well as sticky orbits in the outer regions of specific 3D bars (Chaves-Velasquez et al. 2017) seems to favor the appearance of boxy features in the inner and outer regions of the bars respectively. Sticky chaotic orbits have been also found to shape the bars in studies of 2D models (Patsis et al. 1997; Athanassoula et al. 2010).

The question that we try to answer in this paper is whether or not there are families of periodic orbits (other than the x1-tree set of families) that are associated with the reinforcement of the bar and, in particular, of the morphological features we observe in their central parts (i.e. peanuts and X features embedded in them). For this purpose we study the “*deuxième genre*” periodic orbits in Ferrers bars<sup>3</sup> and we compare their morphologies to those appearing in the papers mentioned at the beginning of the introduction. We do not intend to present in detail the orbital properties of the families. We rather want to point to their origins and discuss whether they could in principle be part of the skeletons of the bars. In order to trace the  $E_J$  at which a *mul*-periodic family is “born”, we follow the evolution of the stability indices of x1, as we did in previous works (Skokos et al. 2002a, PKa,b etc.). For the purposes of the present paper, however, we follow the rules described earlier, and consider x1 each time as *mul*-periodic. We list all the families we found in this way in tables, and we note that their vast majority is presented for the first time. The few cases that correspond to families of p.o. known from earlier works, are accordingly indicated in these tables.

This is the first in a series of papers about the orbital content of galactic bars, in which our main goal is to point out the origin of the various patterns and locate the energies at which they are introduced relatively to the main radial and vertical  $n : 1$  resonances and especially relatively to the vILR. In Section 2 we describe the model, the particular set of parameters we have chosen and the nomenclature we use for the orbits. In Section 3 we present the main 2- and 4-periodic orbits, in Section 4 the main 3- and 6-periodic ones, while in Section 5 we investigate the role of *mul*-periodic orbits with large energies in determining the structure of the bar. Finally in Section 6 we present and discuss our conclusions.

In Appendix A we present morphologies appearing in quasi- and non-periodic orbits and we discuss extensively their similarity with orbits recently found in many models in the relevant literature. These models are either analytic, or have been obtained from snapshots of N-body simulations. In the Appendix we do not present any further new family of periodic orbits, but we compare orbital patterns and we suggest connections between the shapes of published non-periodic orbits and the *mul*-periodic orbits we present in the tables in the main body of the paper. However, readers who just want to read the bottom line of our work should concentrate on Sections 3, 4, 5 and 6, or even go directly to Section 6.

<sup>3</sup> These ellipsoids have been already presented in the 19<sup>th</sup> century by Ferrers (1877) and have been used extensively in Galactic Dynamics, first introduced by Athanassoula et al. (1983).

## 2 INTRODUCING THE MODELS AND THE ORBITS

### 2.1 models

For the sake of continuity with our previous studies on the subject, we use again in this paper the popular triaxial Ferrers bar model, which is described in detail in Skokos et al. (2002a) and Patsis & Katsanikas (2014a), with parameters close to those in the pioneer paper by Pfenniger (1984). The formulae for the axisymmetric part of the potential, as well as the bar model can be found in these references.

The Ferrers bar is inhomogeneous with index 2. He have taken as its major axis our y-axis and axial ratios  $a : b : c = 6 : 1.5 : 0.6$  ( $a, b, c$  are the semi-axes with  $a > b > c$ ).

The axisymmetric background consists of a Miyamoto disc (Miyamoto & Nagai 1975) with fixed horizontal and vertical scale lengths  $A=3$  and  $B=1$  respectively and a Plummer sphere (Plummer 1911) for the bulge with scale length  $\epsilon_s$ .

The length unit is taken as 1 kpc, the time unit as 1 Myr and the mass unit as  $2 \times 10^{11} M_\odot$ . The masses of the three components satisfy  $G(M_D + M_S + M_B) = 1$ , where  $M_D$  is the total mass of the disc,  $M_S$  the mass of the bulge (spheroid),  $M_B$  is the mass of the bar component and  $G$  the gravitational constant.

In all papers mentioned in the beginning of this section one can find detailed descriptions of the components of the models and their properties, so we skip this information here.

### 2.2 Radial and vertical perturbations and the choice of convenient parameters

In this paper we use two specific models, both following the description in the previous subsection, but with different values for the parameters. The first one, used only briefly in this subsection, is the fiducial model of Skokos et al. (2002a), i.e. has  $GM_D = 0.82, GM_S = 0.08, GM_B = 0.1, \epsilon_s = 0.4$ . The frame of reference rotates with the bar pattern speed  $\Omega_p = 0.054$ , which places corotation at a radius  $R_c = 6.13$  from the center.

By searching for the morphologies of the orbits in the papers mentioned in the introduction, we realized that an orbit frequently encountered in the fiducial and in many other Ferrers bar models we have investigated (see e.g. Patsis & Katsanikas 2014a) was the planar orbit depicted in Fig. 1a. In this and in all subsequent plots with orbits the numbers in the axes refer to kpc. In the plots of orbits, usually in the upper left corner, we indicate the depicted projection. The orbit in Fig. 1a belongs to a known family of p.o. that is introduced in the system at the first tangency of the *radial* stability index of the simple-periodic x1 family with the  $b = 2$  axis and thus it is 2-periodic. This family has been discussed in PKb (figure 2 in that paper) and has two branches named rm21 and rm22, because it comes in pairs symmetric with respect to the major axis of the bar. On the  $(x, p_x)$  Poincaré surfaces of sections one can always observe two sets of stability islands belonging to these orbits. For example Fig. 1b depicts the surface of section of the fiducial model for  $E_J = -0.348$ , i.e. an energy right after the bifurcation of rm21 and rm22 from x1. The x1 p.o. is located in the middle of the central stability island, at  $(x, p_x) \approx (0.138, 0)$ , while the two sets of islands in its immediate neighborhood belong to rm21 (left and right of x1) and rm22 (above and below x1, plotted in red). If we plot together both members of this family in the same figure, we observe a rather boxy shape (see figure 2 in Patsis & Katsanikas 2014b, and also Section 3 below).

The families rm21 and rm22 are important and play a major

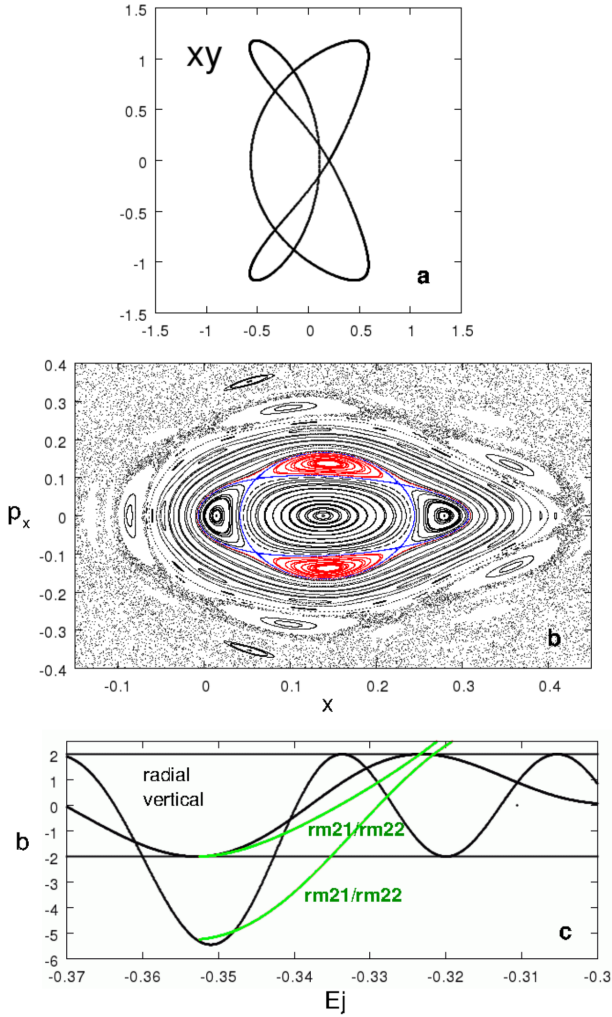


**Figure 1.** (a) A portrait of an  $rm22$  orbit in the fiducial model of Skokos et al. (2002a). (b) The  $(x, p_x)$  Poincaré surface of section close to  $x1$  at  $E_j = -0.348$  in the same model. (c) The stability curves of  $x1$  (black lines) and  $rm21$  and  $rm22$  (green lines). We observe that for  $E_j = -0.348$  the  $rm21/rm22$  families, sharing the same stability curves, are vertically unstable but radially stable. Thus in (b) they are found in the middle of stability islands coming in pairs, above and below (red) and left and right (black) of the central island that belongs to  $x1$ .

role in explaining boxiness in the central region of the bar (Patsis & Katsanikas 2014b; Chaves-Velasquez et al. 2017). Similar morphologies are also encountered in the face-on views of the orbits in figure 7 (third and fourth row) in GLA, in figure 2 in KPP, in figure 4 (1st row) in VSAD and in figure 5 (third column) in WAM. We come up against this morphology almost in all studies about orbits in rotating galactic bars.

In Fig. 1c we give the stability diagram of the  $x1$  family described twice, i.e. when we consider it as being 2-periodic. The stability indices of  $x1$  are plotted with black lines. Arrows indicate which curve corresponds to the radial and which one to the vertical index. Bifurcations of equal multiplicity will occur at tangencies or intersections of the stability curves with the  $b = -2$  axis and will be 2-periodic in this case. We observe that  $rm21$  and  $rm22$  are bifurcated at  $E_j \approx -0.353$  (green stability curves) at the tangency of the  $x1$  radial stability curve with the  $b = -2$  axis. Both share the same stability curves, thus both are bifurcated as simple unstable

**Table 1.** The parameters of the main model.  $G$  is the gravitational constant,  $M_D, M_B, M_S$  are the masses of the disk, the bar and the bulge respectively,  $\epsilon_s$  is the scale length of the bulge,  $\Omega_b$  is the pattern speed of the bar.

| $GM_D$ | $GM_B$ | $GM_S$ | $\epsilon_s$ | $\Omega_b$ |
|--------|--------|--------|--------------|------------|
| 0.878  | 0.1    | 0.022  | 0.4          | 0.054      |

and then they have a  $U \rightarrow S \rightarrow U \rightarrow DU$  transition, in which the stable part  $\Delta E_j \approx 0.012$ . The fact that the pair of  $rm21$  and  $rm22$  is simple unstable does not contradict the presence of invariant curves around it in Fig. 1b. Its radial index is  $-2 < b < 2$  indeed, while the vertical one is  $b < -2$ , starting from the corresponding index of  $x1$ . The  $E_j$  at which  $rm21, rm22$  are bifurcated is in the vILR region, where we have for  $x1$  the  $S \rightarrow U \rightarrow S$  transition, roughly for energies  $-0.36$  and  $-0.342$ , at which first the  $x1v1$  and then the  $x1v2$  families are introduced in the system (Skokos et al. 2002a). This means that vertical perturbations of  $rm1,2$  will correspond mainly to orbits belonging to a chaotic sea, so it would be difficult to compare the side-on morphologies with those presented in the relevant literature. Such issues can be raised in several models and that led us to seek a Ferrers bar model in which the basic families under discussion existed and were introduced as stable. Thus, we performed a preliminary investigation of the energies at which the main 2-, 3- and 4-periodic families are introduced. We have chosen to present the basic  $mul$ -periodic families encountered in rotating 3D bars in a model close to the fiducial one, which however has  $GM_S = 0.022$  instead of  $GM_S = 0.08$ . Thus, as both the mass of the bar and the total mass of the system remain constant, the disc mass increases. The parameters of the main model of this paper are summarized in Tab. 1. In models with bars heavier than that of the fiducial (see figure 3 in Patsis & Katsanikas 2014b), as well as in models with heavier classical bulges, the  $rm21, rm22$  families start existing between the bifurcating points of  $x1v1$  and  $x1v2$ , as vertically unstable.

Useful quantities for assessing the role of the orbits we discuss in the following sections are the  $(E_j, y) = (-0.197, 6.2)$  coordinates on the characteristic diagram of the unstable Lagrangian point  $L_1$  for  $x = 0$  and the  $(E_j, x) = (-0.193, 5.9)$  coordinates of the stable Lagrangian point  $L_4$  for  $y = 0$ . We also note that the longest  $x1$  orbit reaches  $y = 4.1$  kpc along the major axis of the bar.

### 2.3 Orbital nomenclature

Families commonly used in previous studies – such as  $x1, x1v1$ , etc. – already have a name so we keep it also in the present study. In the tables in which we classify the p.o. (sections 3 and 4) we give, for reasons of continuity and clarity, in parenthesis also the name that these families would have if we followed the rules we describe below. In the text, however, we give only the standard name, for brevity.

For the remaining families, we introduce the following nomenclature: The first character indicates whether the family is introduced in a radial (r) or a vertical (v) bifurcation of the  $x1$ . This is followed by two characters indicating its multiplicity, e.g.  $m2$  or  $m3$ , and a third character which is a number giving the order in which this family is introduced in the system. For the unstable counterparts of the stable  $mul$ -periodic families that are bifurcated at the same energy, we add a “u” at the end of the name, retaining the rest of it identical. So e.g. the name  $rm21$  indicates that this is the first radial bifurcation of  $x1$  of multiplicity 2. This family is

bifurcated together with the rm22 family, with which it shares the same stability curves and the orbits of which are symmetric of the rm21 orbits with respect to the y-axis. At the same energy we also have the bifurcation introducing the pair of rm21u and rm22u families, which are the unstable counterparts of rm21, rm22. Since we need a name mainly to associate it with a certain morphology, the clarification is finally done in our Tables, where names and morphologies are presented side-by-side.

Note that a family of multiplicity *mul* will appear also as *2mul*, *3mul* etc. Thus, we keep for the latter the name of the lowest multiplicity with which the family is encountered in the stability diagrams, in order to avoid multiple names for the same family.

Finally, we note that we found only very few important vertical or radial bifurcations from the x1-tree families. So there was no need to extend the nomenclature rules to include such orbits. In the few cases we mention in the sections below we used names that clearly show their origin from the parent family. As an example the family r.tv1 indicates that it is the first vertical bifurcation in the set of radial 3:1 bifurcating from x1 families, for which we used in previous papers names starting with “t” (Skokos et al. 2002a).

In many studies a family is named by the ratio of its frequencies, either in Cartesian or cylindrical coordinates. Although this is often quite adequate for many dynamical studies, it is definitely inadequate for orbital structure work, as several families with quite different properties (such as energy ranges, stability, extents and shapes) have the same frequency ratios. Even naming the orbital families just by the name of the resonance at which they appear, as is usually done for rotating disks, might lead to ambiguities. A good example is that of the x1 and x2 families, both of which would, by the above definition, be named 2:1. We have thus refrained from using names based on frequencies and/or resonances here.

### 3 2-PERIODIC ORBITS

Having chosen a convenient model – i.e. a model in which the rm21/rm22 families exist, are bifurcated as stable and span a sufficient extent – we proceed with finding the families of periodic orbits. In our study we restrict ourselves to the bifurcations of x1 and we do not include bifurcations of the z-axis family (Heisler et al. 1982), as these are not relevant to our study. In order to present the orbits in an illustrative way, we consider the family x1 as 2-periodic and we obtain the stability diagram given in Fig. 2, which shows the origins of all families we discuss in Section 3. We avoid giving the evolution of the stability indices of all these families in Fig. 2 or in separate figures, because we focus mainly in the succession in which these families are introduced in the system. The extent of the families and their possible interesting bifurcations, are discussed whenever they play a role. Moreover we restrict ourselves to a large extent in presenting the families, whose size and shape could make them potential contributors to the bar.

The main 2-periodic families that could play a role in building side-on peanut structures are summarized in Table 2. In our presentation we give only one representative of each family. However, given the 4-fold symmetry of our adopted potential, there exist also symmetric orbits, like e.g. the “frown” and “smile” orbits of the x1v1 and x1v1’ pair, which are symmetric with respect to the equatorial plane. The role of symmetric orbits in building observed structures will be discussed in Sect. 6. Whenever we give initial conditions we give the  $(x, z, p_x, p_z)$  array, since we use the  $y = 0$  surface of section. Numbers in initial conditions are given in the text at least with a three decimal digits accuracy, so that the or-

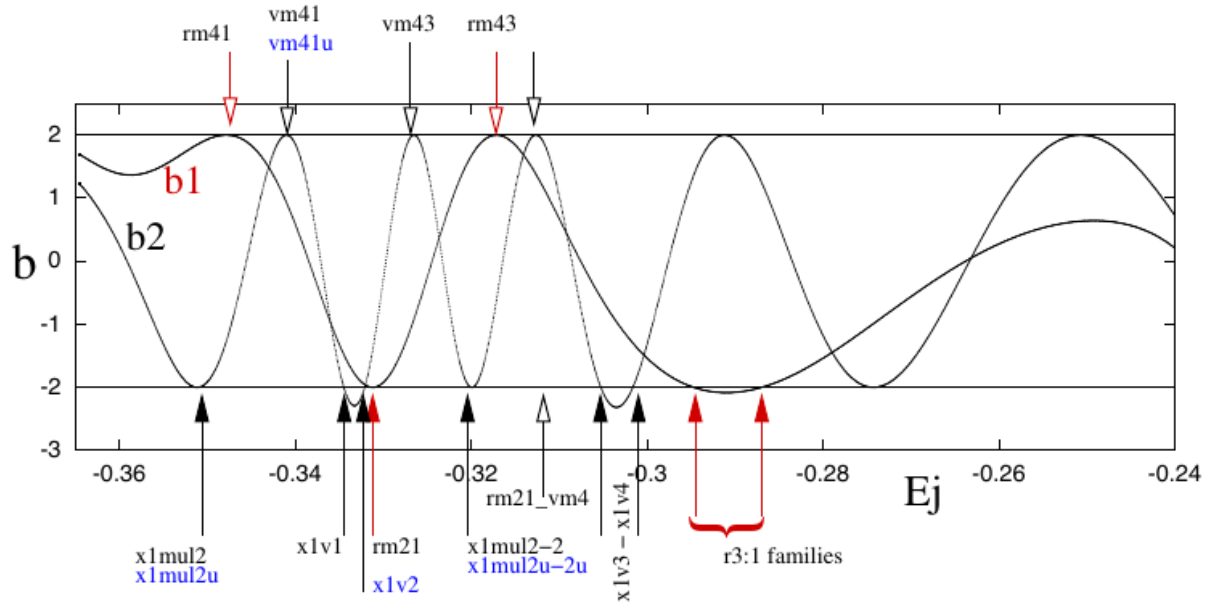
bit can be easily recovered with an iterative scheme. In the present study the p.o. are considered to be found when the initial and final coordinates coincide with an accuracy of at least  $10^{-11}$ , using a fourth order Runge-Kutta method. The relative error in the energy is always less than  $10^{-15}$ .

Table 2 includes all data we need in order to assess the role of each family in a compact manner. In the first column we mention the name with which we refer to the family in our analysis, while in the second column the main information given is the energy  $E_J^*$ , at which the family is born (cf. with Fig. 2). We also add some description about the evolution of the stability of the family. The most important columns are the three that follow, where one can directly associate successively the face-on, end-on and side-on projections of the orbits with the name given in the first column. Stable orbits are plotted in black, while unstable ones in blue. Finally in the last column, we give information about the specific representative of the family depicted in the third, fourth and fifth columns. We give its energy and approximate initial conditions. We always chose a representative of the family that is characteristic over a large  $\Delta E_J$  interval. For example if a family supports a specific face-on profile for a large energy interval, we will present it at an energy within this interval, away from the bifurcating point, where it will be x1-like anyway. Also in the last column we give reference to other works, where similar morphological patterns appear. For the main papers we compare our study with, we use the abbreviations defined in the introduction. Indicating that a p.o. orbit in Table 2 is “similar” to an orbit found in the literature, we mean that itself, or a quasi-periodic orbit in the immediate neighborhood within its stability island, or a chaotic orbit sticky to it (Contopoulos & Harsoula 2008), can be considered as morphologically similar to the orbit in the cited paper. We included only examples where we have conspicuous similarities. However, there are more cases that could be included if we take into account changes that appear as we move along the characteristic of a family (cf. for example the orbit rm21u with the face-on view of the orbit in figure 11 in Deibel et al. 2011).

The orbits are presented in order of increasing  $E_J^*$  from the top to the bottom of the tables (cf. with Fig. 2). The bifurcations of the bifurcating families do not play in general a major role. In the tables we include only those that we find that could be important for supporting the 3D bar structure. In such a case they are given below the parent family separated by a dashed line (see the case of family rm21.vm4 in Table 2).

Special mention has to be given to the group of 3:1 orbits that one can start tracing at the S→U transition of x1 at  $E_J^* \approx -0.295$  (indicated with “r3:1” in Fig. 2). It includes families with stable and unstable parts and face-on morphologies similar to the p.o. t1, t2 and o1 in Skokos et al. (2002a). The tree of 2D and 3D families starts with a *radial* inverse bifurcation (Contopoulos & Magnenat 1985) and extends towards larger as well as towards smaller energies than its  $E_J^*$ , with branches joining again the x1 as well as the x4 characteristics. The interconnections of all their stability curves are complicated and a detailed description is beyond the scope of the present paper. We restrict ourselves to the presentation of a representative of a 3D family with stable parts, which is given in Table 2 with the name r.tv1, mainly because of its side-on profile. This profile could be possibly used for building boxy or X-shaped side-on projections.

In Table 2 we have also included the simple periodic (of multiplicity 1) x1v1 and x1v2 families, as essentially the contribution of all the remaining families is discussed in comparison with the edge-on profiles that can be built by mechanisms using these two families as building blocks. It has to be added that in the particular model we



**Figure 2.** The stability diagram of the  $x1$  family considered as 2-periodic. The index  $b1$  refers to radial, while  $b2$  to vertical perturbations. Red arrows point to the energies at which 2D families are introduced in the system, while black to the corresponding energies for 3D families. Note that the families indicated at the tangencies of the stability curves with the  $b = 2$  axis, are introduced as 4-periodic. The names of the families in blue indicate that they are introduced as unstable.

[h]

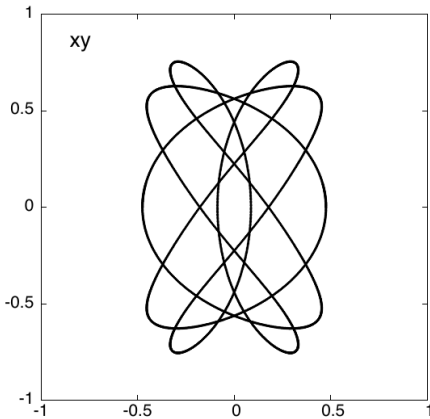


**Figure 3.** The representatives of the families  $rm21$  and  $rm22$  at  $E_j = -0.324$  plotted together. They can obviously be the backbone for boxy features in the regions they exist.

use for the presentation of the orbits, the  $x1v1$  family does not have complex unstable parts, as in all other known cases up to now, thus its role for building an X-feature can in principle be based solely on quasi-periodic orbits trapped around stable p.o. This fact upgrades the role of  $x1v1$  and  $x1v2$  families as peanut building blocks and deserves further investigation, since the parameter that differentiates the specific model we use for the presentation of orbits here with respect to other Ferrers bar models, is the increase of the disc mass at the expense of the bulge’s mass.

The easiness with which a pattern is encountered in different models is reflected in the number of works in which it is found and mentioned in the last column of Table 2. This can be used as a rule of thumb for the importance of each morphological pat-

tern. The large frequency with which the pairs of  $rm21/rm22$  and  $rm21u/rm22u$  are encountered in the studies is a result of the phase space structure of the  $x1$  stability islands in the inner parts of any rotating bar model. The  $(x, p_x)$  Poincaré surface of section given in Fig. 1b is typical of the situation. The islands of the multiplicity 2 orbits surround invariant curves around  $x1$ , they occupy a considerable area of the large  $x1$  stability island and they are located in a zone with orbits that have relatively small deviations from the initial conditions of the  $x1$  p.o. Furthermore, their shape is indicative of the morphology of the quasi-periodic orbits one can find on the neighboring invariant curves (see also Section A). The  $rm21/rm22$  pair offers also a characteristic image of the skeleton of the orbits that shape inner boxiness in models of bars. The pattern resulting when both  $rm21$  and  $rm22$  are considered in our model is given in Fig. 3 (cf with figure 2 in PKb). We have however, to bear in mind that these orbits cannot be used for shaping the overall structure of the bar. Bifurcated from  $x1$ , they start increasing their projections on the minor and decreasing their projections on the major axis of the bar. As the energy, and thus their perimeter, increases, they develop loops that extend to the sides of the main ellipse. Namely, with increasing energy we have an evolution in the direction from the  $rm21$  orbit depicted in Table 2 to the  $(x, y)$  projection of  $rm21\_vm4$  given just below it in the same table. Its stable part along its characteristic, together with that of its bifurcating families, extends up to  $E_j \approx -0.312$ . At this energy the  $rm21$  and  $rm22$  orbits are already much rounder than the orbits in Fig. 3. Their maxima along the  $x$ - and  $y$ -axes evolve from  $(x_{max}, y_{max}) = (0.18, 0.72)$ , to  $(0.47, 0.75)$ , to  $(0.68, 0.79)$  to  $(0.78, 0.78)$  for  $E_j = -0.331, -0.324, -0.316$  and  $-0.312$ , respectively. This morphological evolution, combined with the fact that these orbits are generated at the ILR region, relates them directly with the effect of inner boxiness observed in many barred galaxies (Athanassoula & Beaton 2006; Erwin & Debattista 2013), in agreement with results of previous studies (PKb, Chaves-Velasquez et al. 2017).

**Table 2.** The main periodic orbits bifurcated from the  $x1$  family considered as being 2-periodic (Fig. 2). The successive columns give the name of the family, following the rules described in Sect. 2.1 (1), the energy at which it is introduced in the system ( $E_J^*$ ) and information about its stability (2), the face-on, end-on and side-on views (3-5), while in the last column (6), labeled “comments”, we give the  $E_J$  value of the specific orbit plotted, its approximate  $(x, z, p_x, p_z)$  initial conditions and we mention figures in papers in which similar morphologies are presented. From top to bottom, the families are given in order of increasing energy at which they are introduced in the system. Bifurcations of the families, if given, are separated from the parent family with a dashed line. Orbits drawn with black (blue) lines are stable (unstable).

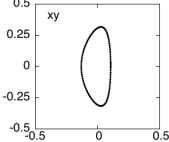
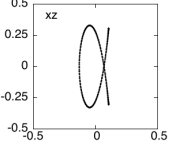
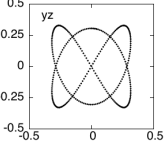
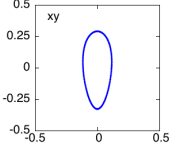
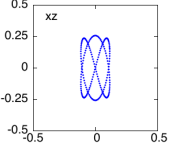
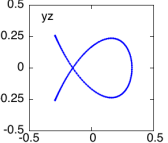
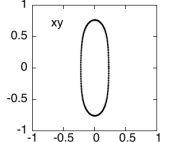
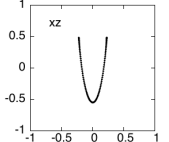
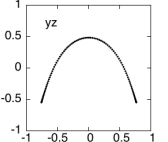
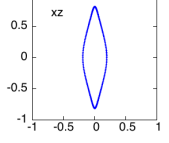
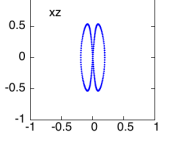
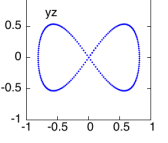
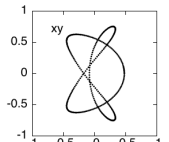
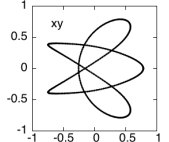
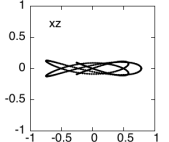
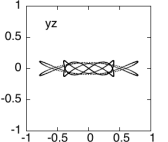
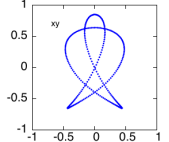
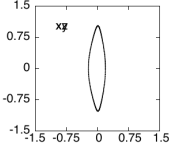
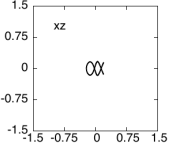
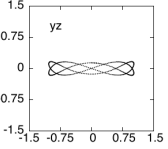
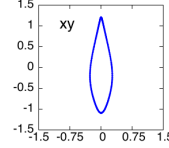
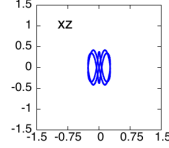
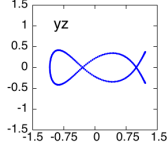
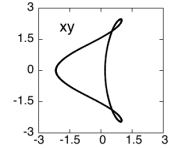
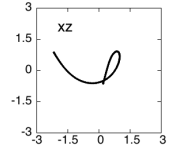
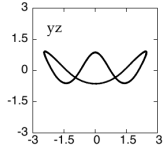
| family name                | $E_J^*$  | face-on   | end-on  | side-on   | comments   |
|----------------------------|--|---|---|---|--|
| <b>x1mul2<br/>(vm21)</b>   | -0.351<br>(1st tangency of $b2$ with the $b = -2$ axis). S for $E_J < -0.283$ .  |    |    |    | $E_J = -0.333$<br>(0.107, 0.305, 0, 0)<br>Figure 16 top in PKb.  |
| <b>x1mul2u<br/>(vm21u)</b> | -0.351<br>(1st tangency of $b2$ with the $b = -2$ axis). U always. Radially stable for $E_J < -0.292$ .  |    |    |    | $E_J = -0.34$<br>(0.115, 0.167, 0.008, -0.109)<br>Side-on view similar to figure 2, top, in PWG.   |
| <b>x1v1<br/>(vm11)</b>     | -0.334<br>1st vILR (frown-smile) family. S always (no $\Delta$ part in this model).  |    |    |    | $E_J = -0.3$<br>(0.2240, 483, 0, 0)  |
| <b>x1v2<br/>(vm11u)</b>    | -0.332<br>2nd vILR ( $\infty$ -type) family. U always, being radially stable.  |   |   |   | $E_J = -0.3$<br>(0.193, 0, 0, 0.275)   |
| <b>rm21</b>                | -0.331<br>(1st tangency of $b1$ with the $b = -2$ axis). S for $E_J < -0.316$ .  |  |   |   | $E_J = -0.324$<br>(0.475, 0, 0, 0)<br>Figure 2 in PKb; similar to face-on views of orbits in figure 7 (3rd and 4th rows) in GLA, figure 4 (1st row) in VSAD, figure 5 (third column) in WAM. |
| <b>rm21_vm4</b>            | -0.315<br>4-periodic, 3D bifurcation of $rm21$ at an intersection of $b2$ index of $x1$ with the $b = -2$ axis. S: $E_J < -0.311$ . Found as U, DU also at smaller $E_J$ (regression of characteristic). |  |  |  | $E_J = -0.311$<br>(0.781, 0, 0, 0.048)<br>Face-on view as for $rm21$ .   |
| <b>rm21u</b>               | -0.331<br>(1st tangency of $b1$ with the $b = -2$ axis). Initially U for $E_J < -0.316$ . Then S towards smaller $E_J$ .   |  |   |   | $E_J = -0.323$<br>(0.381, 0, 0.102, 0)<br>Similar to face-on views of orbits in figure 7 in GLA, figure 4 in VSAD and figure 5 in WAM.   |

Table 2 – *continued*

| family name   | $E_J^*$   | face-on   | end-on  | side-on   | comments   |
|---|---|---|---|---|--|
| <b>x1mul2-2</b><br>( <b>vm23</b> )  | -0.320<br>(2nd tangency of<br>b2 with the $b =$<br>$-2$ axis).<br>S: $E_J < -0.236$   |  |  |  | $E_J = -0.316$<br>(0.196, 0.135, 0, 0).<br>Boxy side-on<br>view. |
| <b>x1mul2-2u</b><br>( <b>vm23u</b> )  | -0.3<br>(2nd tangency<br>of b2 with the<br>$b = -2$ axis). Initially U. S parts<br>for $E_J > -0.235$ .   |  |  |  | $E_J = -0.316$<br>(0.196, 0.135, 0, 0).                          |
| <b>x1v3 and x1v4</b> as 2-periodic (see figures 9 and 10 respectively in Skokos et al. 2002a) |   |   |   |   |  |
| <b>r.tv1</b>  | -0.295 (starting<br>point - inverse<br>bifurcation)<br>(1st intersection<br>of b1 with the<br>$b = -2$ axis).<br>A group of S,<br>U families with<br>triangular face<br>on views and their<br>radial and vertical<br>bifurcations<br>extending also to<br>lower $E_J$ . |  |  |  | $E_J = -0.2299$<br>(0.190, -0.635, 0, 0).                        |

Finally, the 4-periodic orbits are summarized, in the same way as the 2-periodic ones, in Table 3. We observe that the projections of all *mul*-periodic orbits have a morphology that can be described as a Lissajous figure, which becomes more complicated as the energy, at which a family is bifurcated increases. This is more evident in the side-on projections of the 3D orbits.

#### 4 3-PERIODIC ORBITS

We followed the same approach for tabulating also the 3- and 6-periodic  $x1$  bifurcations. The corresponding stability diagram is given in Fig. 4. Arrows point again to the origin of the families, which are included in Tables 4 and 5.

The 3-periodic families also offer some patterns that are frequently encountered in orbital analyses of barred galaxies models. Among them we find, in a relatively large range of  $\Delta E_J$  values, the face-on view of the *vm35* family and the similar, planar, family *rm33*. This latter family, together with the 2-periodic *rm21* one, appear typically on the  $(x, p_x)$  Poincaré surfaces of section at energies close to the *vILR* region (e.g. figure 1 in PKb). The morphological evolution of *vm35* gives a nice example of how the evolution of a projection of a family changes shapes along its characteristic, influenced by the resonances it encounters. At the bifurcating point, its face-on view is by default  $x1$ -like. However, at larger energies it develops a face-on morphology similar to *rm33*, in the same way as the  $x1$  orbits on the equatorial plane change their morphology along their characteristic by developing locally three apocenters at the 3:1 resonance region, four at the 4:1 resonance etc. We can say that the shape of the orbits along a characteristic of a family “feels”

the resonance it passes by at the corresponding  $\Delta E_J$  regions. Thus, the *rm33* face-on pattern becomes more important for the overall dynamics of the system, as it can be also encountered at larger energies on the characteristic of one more, 3D now, family. The 3D *vm35* family in turn, bifurcates at  $E_J = -0.3087$  a 6-periodic 3D family that has edge-on projections with their own morphology and co-exists with the parent family.

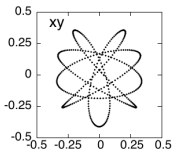
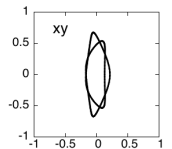
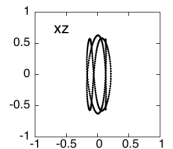
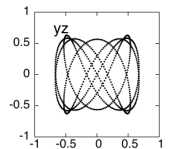
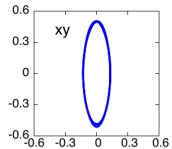
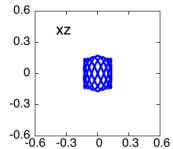
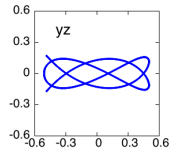
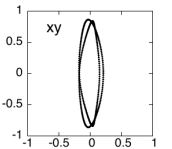
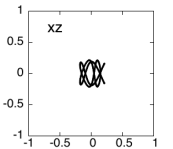
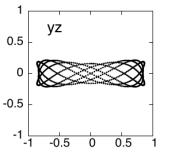
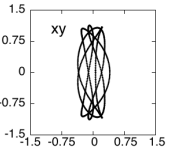
In Table 5, where we present 6-periodic orbits, we meet again families that we have already presented as 2-periodic, at tangencies of the 3-periodic  $x1$  stability curves with the  $b = 2$  axis. Thus, the first to appear in the table is the known *x1mul2* family, while at a larger energy in the stability diagram of Fig. 4, we meet again *rm21* and *rm22*.

For the 3- and 6-periodic orbits, we observe again that the larger the energy, the more complicated, more “dense”, Lissajous figures we have in their edge-on profiles. In most cases of the 3D families in Tables 4 and 5 we have more distinguishable shapes in the side-on profiles of the unstable periodic orbits and on the end-on of the stable ones (a kind of exception seems to be the *vm37* - *vm37u* pair). This means that it is easier for the side-on profiles based on 3- and 6-periodic stable orbits to obtain a compact, boxy, character.

As multiplicity and energies increase, we find profiles of p.o. that resemble more those of 3D quasi-periodic orbits trapped around  $x1$ . Characteristic examples are the side-on projections of the two 6-periodic orbits we present in Table 5, as well as the one of the p.o. *vm43* (Table 3). The local minimum of the  $z$  extent at  $y=0$  in the side-on views of *vm65* and *vm43* is reminiscent of the corresponding minimum of the  $x1$  quasi-periodic orbits on invariant tori approaching the *x1v2* initial conditions (see figure 15 in



**Table 3.** The same as Table 2, now for p.o. of multiplicity 4.

| family name  | $E_J^*$  | face-on  | end-on  | side-on  | comments  |
|--------------|--|--|---|--|---|
| <b>rm41</b>  | -0.348<br>(1st tangency of b1 with the $b = 2$ axis) |   |   |  | $E_J = -0.345$<br>(0.035, 0, -0.137, 0).<br>Similar with face-on view of orbit in figure 6, 2nd row in GLA. |
| <b>vm41</b>  | -0.341<br>(1st tangency of b2 with the $b = 2$ axis) |   |  |  | $E_J = -0.3$<br>(0.128, 0.565, 0, 0).<br>Face-on similar with figure 10, bottom row, in WM-D.               |
| <b>vm41u</b> | -0.341<br>(1st tangency of b2 with the $b = 2$ axis) |   |  |  | $E_J = -0.337$<br>(0.129, 0.129, -0.0009, 0.038).   |
| <b>vm43</b>  | -0.326<br>(2nd tangency of b2 with the $b = 2$ axis) |   |  |  | $E_J = -0.32$<br>(0.2080, 0.158, 0, 0).   |
| <b>rm43</b>  | -0.317<br>(2nd tangency of b1 with the $b = 2$ axis) |  |   |  | $E_J = -0.315$<br>(0.064, 0, 0, 0).<br>Similar with face-on view of orbit in figure 6, last row, in GLA.    |

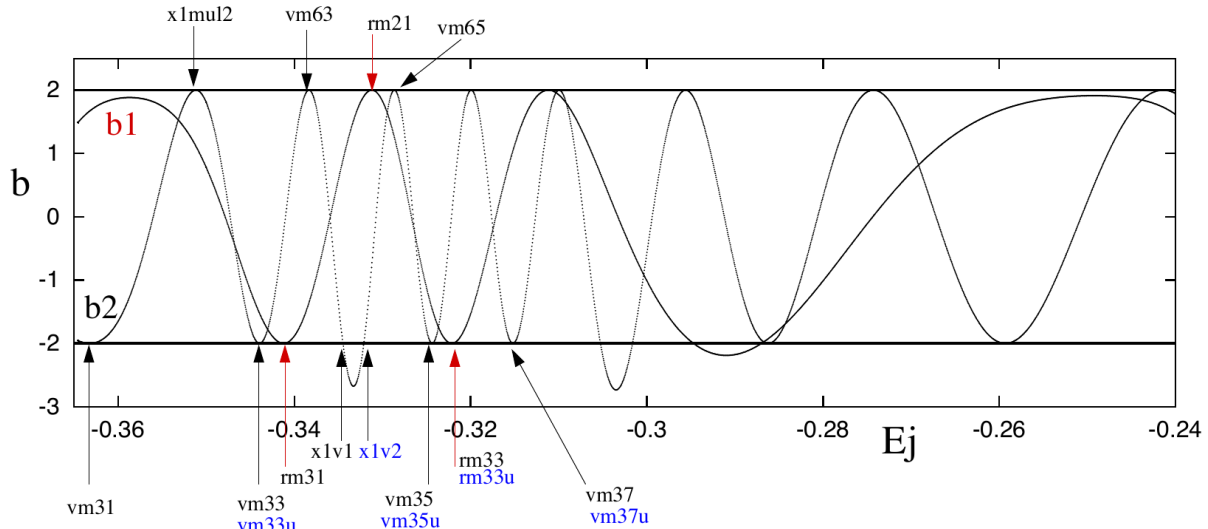


**Figure 4.** Stability diagram for  $x_1$  considered as 3-periodic. Arrows and colors as in Fig. 2.

PKa), while the side-on view of vm63, having a local very shallow maximum at (0,0), points to side-on profiles of 3D quasi-periodic orbits of  $x_1$  approaching the energy at which  $x_1v_1$  is bifurcated (figure 2 in PKa). Such orbits have to be counted among those that reinforce peanut-shaped morphologies.

For the sake of completeness we have calculated the families

of 5-periodic orbits as well. We do not present them here separately, since their edge-on morphologies can be simply described as “boxy”, complicated Lissajous figures. They are found combined with any kind of face-on morphologies presented in the tables, from  $x_1$  ellipses to rather “filled” shapes (cf for example the face on views of vm41u or vm43 with rm43 in Table 3).

**Table 4.** The same as Table 2, now for p.o. of multiplicity 3.

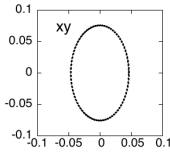
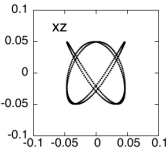
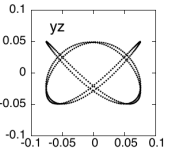
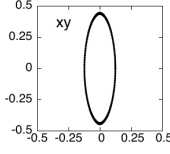
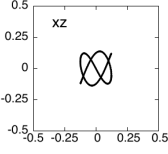
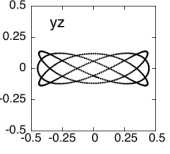
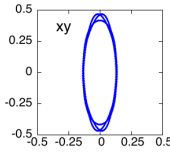
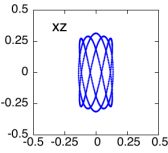
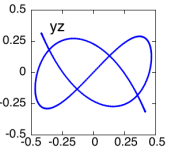
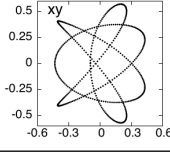
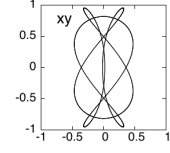
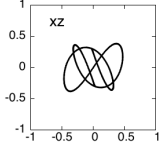
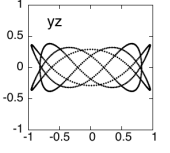
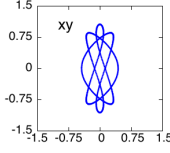
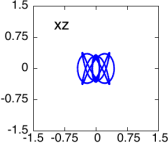
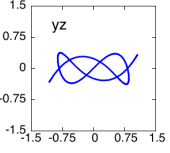
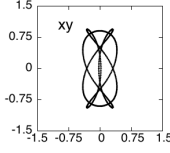
| family name                        | $E_J^*$  | face-on   | end-on  | side-on  | comments  |
|------------------------------------|--|---|---|--|---|
| <b>vm31</b>                        | -0.363<br>(1st tangency of<br>b2 with the $b = -2$ axis)   |    |    |    | $E_J = -0.362$<br>(0.046, 0.049,<br>-0.0007, -0.003).   |
| <b>vm33</b>                        | -0.344<br>(2nd tangency of<br>b2 with the $b = -2$ axis)   |    |    |    | $E_J = -0.341$<br>(0.124, -0.058,<br>-0.001, -0.073).   |
| <b>vm33u</b>                       | -0.344<br>(2nd tangency of<br>b2 with the $b = -2$ axis)   |    |    |    | $E_J = -0.330$<br>(0.130, -0.229,<br>0.006, -0.091).<br>side-on view<br>similar with<br>figure 6, last<br>row in AVSD,<br>figure 2, 3rd row<br>and figure 5 down<br>in PWG,<br>figure 4 last row<br>in VSAD, fig-<br>ure 21 2nd and<br>3rd columns in<br>WAM. |
| <b>rm31</b>                        | -0.341<br>(1st tangency of<br>b1 with the $b = 2$<br>axis)   |  |   |  | $E_J = -0.333$<br>(-0.091, 0, 0, 0).  |
| <b>x1v1 and x1v2 as 3-periodic</b> |  |   |   |  |   |
| <b>vm35</b>                        | -0.324<br>(3rd tangency of<br>b2 with the $b = -2$ axis)<br>S: $E_J < -0.304$ .  |  |  |  | $E_J = -0.305$<br>(0.358, -0.187,<br>0.105, 0.143).<br>Face-on similar<br>with figure 4 in<br>PKb and with<br>figure 7, last row,<br>in GLA.  |
| <b>vm35u</b>                       | -0.324<br>(3rd tangency<br>of b2 with the<br>$b = -2$ axis)<br>Initially (and<br>mostly) U, Small<br>S and $\Delta$ parts<br>close to $E_J$<br>$\approx -0.28$ |  |  |  | $E_J = -0.307$<br>(0.127, -0.239,<br>0.087, -0.096).  |
| <b>rm33</b>                        | -0.322<br>(2nd tangency of<br>b1 with the $b = 2$<br>axis)   |  |   |  | $E_J = -0.318$<br>(-0.0257, 0, 0, 0).<br>Same with orbit<br>in figure 4 in<br>PKb, similar with<br>orbit in figure 7,<br>last row, in GLA.  |

Table 4 – continued

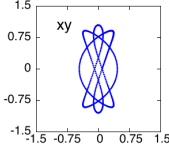
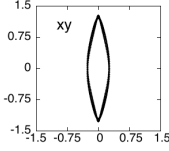
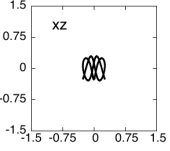
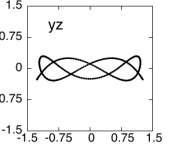
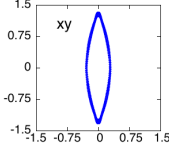
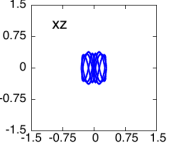
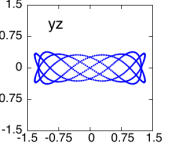
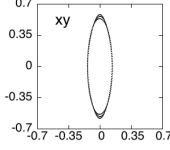
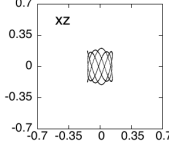
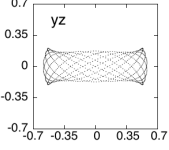
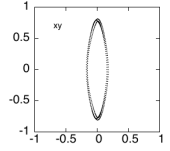
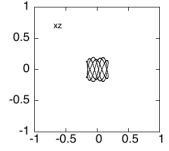
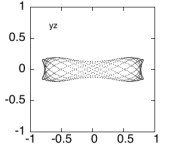
|              |  |   |   |  |   |
|--------------|--|---|---|--|---|
| <b>rm33u</b> | -0.322<br>(2nd tangency of<br>b1 with the $b = 2$<br>axis)                   |  |   |  | $E_J = -0.317$<br>(0.0916, 0, 0, 0).                  |
| <b>vm37</b>  | -0.315<br>(4th tangency of<br>b2 with the $b =$<br>-2 axis)<br>S in general. |  |  |  | $E_J = -0.304$<br>(0.262, 0.112,<br>-0.012, -0.127).  |
| <b>vm37u</b> | -0.315<br>(4th tangency of<br>b2 with the $b =$<br>-2 axis)<br>U in general. |  |  |  | $E_J = -0.298$<br>(0.278, -0.258,<br>-0.157, -0.096). |

Table 5. The same as Table 2, now for p.o. of multiplicity 6.

| family name                    | $E_J^*$  | face-on   | end-on  | side-on  | comments   |
|--------------------------------|--|---|---|--|--|
| <b>x1mul2 as 6-periodic</b>    |  |   |   |  |  |
| <b>vm63</b>                    | -0.338<br>(2nd tangency of<br>b2 with the $b = 2$<br>axis) |  |  |  | $E_J = -0.333$<br>(0.131, 0.140,<br>-0.0035, 0.061).<br>Similar to x1<br>quasi-periodic<br>orbits, figure 6 in<br>PKa. |
| <b>rm21/rm22 as 6-periodic</b> |  |   |   |  |  |
| <b>vm65</b>                    | -0.328<br>(3rd tangency of<br>b2 with the $b = 2$<br>axis) |  |  |  | $E_J = -0.24$<br>(0.173, 0.105,<br>0.001, 0.066).<br>Similar to x1<br>quasi-periodic<br>orbits, figure 15<br>in PKa.   |

## 5 MULTI-PERIODIC, QUASI- AND NON-PERIODIC ORBITS AT HIGH ENERGIES

Bifurcations introduce complexity in a dynamical system. In our rotating bar model the families bifurcated from the x1 family have more complicated morphologies than those of the x1 p.o., because they develop asymmetries or loops. This results generally to shapes that are less elongated than those of the x1 ellipses at the same energy (e.g. the 3:1-type bifurcations). This is particularly the case for the shapes of the *mul*-periodic orbits, whose outline become evidently “rounder” than the x1 already at energies close to the one at which they have been bifurcated. The effect is more conspicuous in the projections of the 3D bifurcations of x1 on the equatorial plane.

In the particular Ferrers bar model we use in this work, the x1 characteristic and stability curves do not have a smooth evolution at high energies. They are characterized by foldings and “bows” respectively (Skokos et al. 2002a). At any rate, the longest x1 p.o. reaches a  $y \approx 4.1$  value, which can be considered as an estimation of the maximum radius of the bar we can build with the or-

bit content of this model. At high energies, the “round” shapes of the x1 bifurcations, and especially those of the *mul*-periodic ones, spread out beyond the extent of the x1 in the direction of the bar minor axis. Thus they can not be part of the bar. Since they are not elongated along the major axis of the bar, the only way to contribute to its density would be to build substructures *within* the bar. We give in Fig. 5 typical p.o. that dominate the outer parts of the model and are suitable for describing the situation we refer to. The black ellipse is the x1 p.o. for  $E_J = -0.22$ , close to the longest x1 in the system, while the other three plotted are for  $E_J = -0.2$ . The rectangular-like x1 p.o. is the x1 representative at this energy (plotted with red). It is stable and already considerably square, so it does not help the bar to extend to larger distances from the center. In other models, chaotic orbits, sticky to rectangular-like periodic ones, could support an outer boxiness of the bar (Patsis et al. 1997). In this model such orbits exist in a small  $\Delta E_J$  interval. In any case, this refers essentially to the shape of the outermost x1 p.o. and not to the presence of another orbit, let alone of a *mul*-periodic bifurcation. The rhomboidal, green p.o., typical at the 4:1 resonance of

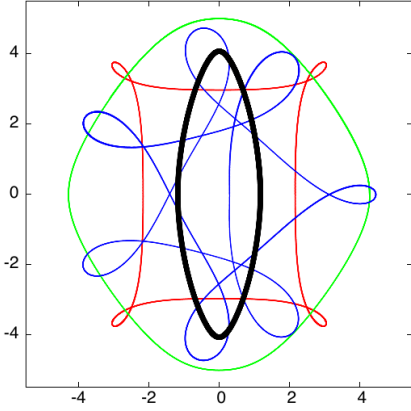


**Figure 5.** Typical periodic orbits at the outer parts of the model. In black we give one of the longest x1 p.o. at  $E_J = -0.22$ , while the three others (red, blue and green) are at  $E_J = -0.2$ . The blue, 3-periodic orbit is typical of the shape of *mul*-periodic orbits we encounter at high energies. Only the x1 p.o. can be considered as bar-supporting.

rotating galactic models, could be associated only with inner rings or perhaps lenses. The blue, 3-periodic orbit at the same energy, could only contribute to the enhancement of a disc surrounding the bar. Evidently, such orbits could not be used as a basis for supporting thick bar structures either. For this reason we do not proceed to a detailed presentation of orbits that are obtained when the radial bifurcations of x1 at high  $E_J$  are vertically perturbed.

As regards the 3D families of the x1-tree, which support the bar, they provide building blocks that stay closer and closer to the equatorial plane as energy increases (Patsis et al. 2002b). They are organized in blocks belonging to stable x1 $\nu$ n families that reach a maximum radius,  $R_{max}$ , on the equatorial plane, beyond which only the height of their individual orbits increases. This maximum radius can be considered as a maximum distance within which these orbits can support the bar. In this way the edge-on view forms a profile with the outline of a staircase (we refer to it as a “stair-type” profile) and in which the larger the  $n$  of the parent x1 $\nu$ n family, the more vertically thin, within  $R_{max}$ , the building block will be (cf figures 11 to 19 in Patsis et al. 2002b). The shapes of their radial bifurcated orbits become “rounder” as  $E_J$  increases, as already noted for the orbits radially bifurcated from x1. However, apart from the round shapes that render them as non-bar supporting, the radial bifurcations of the x1 $\nu$ n families in the model have parts of their characteristic that extend towards the center of the system, bringing members of these families to the central regions. However, none of the encountered morphologies had the dimensions to characterize a face-on or edge-on profile.

As the energy increases, the structure of the phase space of a rotating 3D bar becomes increasingly complex, since the number of existing families of p.o. increases and their stability varies. Chaos increases not only because the volume of the chaotic seas becomes larger, but also because small deviations from the initial conditions of an orbit may bring it on different zones of influence of the numerous p.o. existing at the same energy. In other words the shape of a structure that will be possibly supported is sensitive to the perturbation that we apply. This dependence is clearly non-monotonic. It is technically not easily workable to isolate these zones of influence around the p.o. in the 4D space of section of a 3D system. While we have a fair understanding of the contribution of the 3D families of the x1 tree to the backbone of 3D bars (Patsis et al. 2002b) and

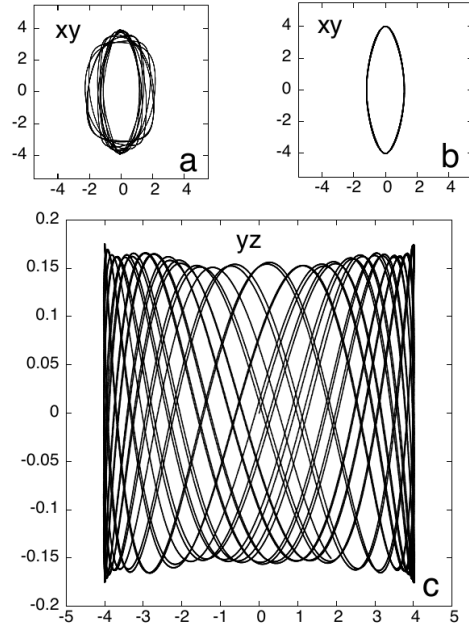


**Figure 6.** Vertically perturbed x1 orbits at  $E_J = -0.22$ . In (a) is given the face-on projection of the orbit perturbed by  $p_z = 0.1$ , while in (b) by  $p_z = 0.05$ . In (c) we give the side-on view of the orbit in (b), with different scale in the axes. This is a profile typical for vertically perturbed x1 orbits.

knowledge of the contribution of quasi- and non-periodic orbits at the ILR regions of the models (Katsanikas et al. 2013, PKa, PKb), less work has been done in assessing the role of 3D quasi- and non-periodic orbits around the planar x1 orbits (Chaves-Velasquez et al. 2017). Here we give in Fig. 6 an example that delineates how a vertically perturbed x1 orbit close to the end of the bar could contribute to the edge-on profile of our model. We consider the x1 orbit at  $E_J = -0.22$ , which we see in Fig. 5 and we start increasing  $p_z$ . The face-on view of the orbit when perturbed by  $p_z = 0.1$  fills a thick ring (Fig. 6a), similar to quasi-periodic orbits obtained when the orbit is perturbed radially. The orbit is on a torus, i.e. viewed edge-on, it has effectively rectangular-like edge-on projections that can be vaguely described as complicated Lissajous figures reaching a height about 0.4 above the equatorial plane. Similar edge-on profiles are obtained for smaller perturbations as well, however the height they reach is much smaller. In Fig. 6b we give the face-on projection of the x1 orbit perturbed by  $p_z = 0.05$ , which is almost identical to the planar x1 orbit. However, its side-on view given in Fig. 6c is again rectangular like. The orbits have been integrated for seven x1 periods. We did not find at large energies any simple *mul*-periodic edge-on morphology like those encountered in the central parts of the model and described in the tables.

By increasing the vertical perturbations even more we do not necessarily enter a chaotic sea. Moving along a direction in phase space we may reach tori of another family. By reaching a perturbation  $p_z = 0.2$  of the x1 orbit of Fig. 5, i.e. by applying a larger vertical perturbation than in the case of the orbits of Fig. 6, we reach a quasi-periodic orbit around x1 $\nu$ 4, which for  $E_J = -0.22$  is stable in our model. Such orbits, if populated, will support a peanut shaped thick bar in which the thick part is almost the bar itself and not part of it as we can observe in Fig. 7 (see also figure 1c in Patsis et al. 2002b). In principle, in our model we can find edge-on profiles that are determined by simple periodic orbits of the x1 tree at high ener-

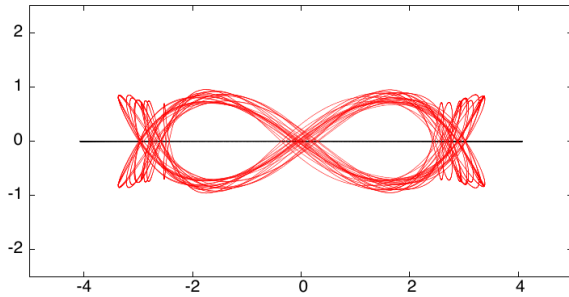


**Figure 7.** The side-on projection of a x1 orbit at  $E_J = -0.22$ , perturbed by  $p_z = 0.2$  that reaches a x1v4 torus. The black horizontal line, indicates the length of x1 at the same energy.

gies. However, *mul*-periodic, vertical, 3D bifurcations of the x1vn families with  $n \geq 3$ , are rather insignificant. In most cases they exist only in narrow  $\Delta E_J$  intervals and their characteristics fall again on the characteristic of the parent family. Thus, at high energies the profiles that dominate are mainly those of complicated Lissajous figures or one of the known shapes of the *simple*-periodic orbits of the x1-tree.

We conclude that the role of *mul*-periodic orbits is reduced as energy increases. Practically, the shapes of the most important *mul*-periodic orbits can play a role only in the thick part of the bar, which in the case we study here, as in most cases of barred galaxy models, ends between 0.3 and 0.7 times the length of the bar (e.g. Fig. 11 in Athanassoula et al. 2015).

The reader interested in the comparison of the orbital shapes published in the papers mentioned in the very beginning of the introduction with the morphology of the periodic orbits presented in the tables, may proceed at this point to Appendix A. In the next section we discuss the main results of our study.

## 6 DISCUSSION AND CONCLUSIONS

We studied here the origin of morphologies appearing in the projections of orbits of multiplicity higher than one and which are not trapped in the immediate neighborhood of the x1 family or of the families of the x1 tree. We investigated the possibility of having bars built with orbits that deviate considerably from elliptical-like morphologies. Our study was motivated by the existence of such orbits, mentioned lately in a number of papers about the orbital content of 3D galactic bars.

The present work is mainly comparative and aims to the understanding of the origin of such orbits and of their shapes, a study sorely missing from all papers presenting and discussing their morphologies. The vast majority of the orbits found in published papers are quasi- or non-periodic. Thus, they can be either trapped on invariant tori around a stable periodic orbit, or they will be diffusing in a chaotic sea. A kind of intermediate situation are the sticky chaotic orbits (see e.g. Contopoulos & Harsoula 2008), in which an ultimately chaotic orbit behaves for a relatively long time as regular, supporting a particular structure. Below, we summarize the basic subjects discussed through our paper and the corresponding main results we reached in each case:

### 6.1 3D Quasi- and non-periodic orbits may combine in their three projections morphologies from projections of different families of p.o:

The morphology of a 3D orbit exhibits in its three projections in general patterns that have been introduced in radial or vertical resonances, at lower energies than the energy of the orbit. This can happen in two ways. Firstly, when a 3D family is bifurcated from a parent one as  $E_J$  increases, it may retain either the edge-on or the face-on morphology of the parent family, depending on whether the radial or the vertical stability index reaches a  $b = \pm 2$  axis, respectively. A new family will have in its projections a combination of old and new features. Secondly, at a certain  $E_J$ , if we start perturbing the initial conditions of a periodic orbit in phase space we will approach those of another p.o. family. By doing so, we observe a smooth, gradual transition from a certain morphology of a quasi- or non-periodic orbit to another morphology. The navigation in the 4D space of section of an autonomous Hamiltonian system has several practical complications. Nevertheless, an example of the smooth variation of the morphology of the orbits as we depart from the initial conditions of a periodic one has been given in PKa. Moving along the  $p_z$  direction from x1 towards x1v2, the 3D quasi-periodic orbits of the stable x1 orbit start resembling in their side-on profiles the unstable x1v2 orbit. When we cross the last invariant torus around x1 and we enter the 4D chaotic sea, the unstable manifold of the x1v2 leads us around the x1v1 tori and then the side-on projections of the orbits exhibit hybrid x1v1-x1v2 morphologies (see figure 12 in Katsanikas et al. 2013, and figure 13 in PKa). Such morphological transformations are typical as one moves in the phase space, although we have not yet established rules to predict them. For the needs of the present paper we keep in mind that the individual morphological patterns presented in the columns of Tables 2 to 5 can be encountered also combined in the projections of quasi- and non-periodic orbits in several models.

### 6.2 About the information included in the Tables with the *mul*-periodic orbits:

Since the detailed discussion of all families bifurcating from the x1-tree and of their evolution would be impractical, we presented the main orbital patterns summarized in Tables. In these Tables we refer to the origin of the various morphological patterns published in several papers. A secure conclusion is that they have their origin in the second type bifurcations of x1. The best way of presenting how they are linked to x1 is to find the tangencies (or intersections) of the stability curves of x1 with the  $b = 2$  and  $b = -2$  axes when it is considered *mul*-periodic. Since x1 is almost everywhere stable, at the tangencies, there are always bifurcated pairs of one initially stable and one initially unstable family. Because of the symmetries in our model, these orbits have also symmetric counterparts with respect to axes of the system. These “twin” orbits share the same stability curves. In practice, the p.o. presented in the tables of the present paper, together with the orbits of the x1-tree in Patsis et al. (2002b), can be considered as the basis for most orbital patterns expected to exist in many standard 3D N-body barred galaxy models.

### 6.3 Where do we find each orbital morphology on the spaces of section?

By comparing the shapes of the orbits in our Tables with the structures of the published orbits in the models, it is obvious that not all orbital patterns are encountered with the same frequency. This may

be due to the fact that the second type bifurcations we study, occupy parts of the stability islands centred on the  $x_1$  p.o., as we can realize in the 2D case of orbits on the equatorial plane (see e.g. Fig. 1b). Such islands have always central parts with invariant curves belonging to quasi-periodic orbits morphologically influenced by the shape of the central p.o. In the case of  $x_1$ , they are elliptical-like. Then, at larger distances from the center of the island, we have, as expected, a ring of smaller islands surrounding the central part. In the case described in Fig. 1b the region of this ring is under the  $rm21/rm22$  and  $rm21u/rm22u$  morphological influence. The area of phase space where the initial conditions of a quasi- or non-periodic orbit with a given morphology will be located is determined by the degree of perturbation of the p.o.

In 3D cases it is more difficult to isolate the areas of morphological influence. It is characteristic that in all cited studies the frown - smiles and “ $\infty$ ”-like profiles are included (in AVSD figure 6, 3rd row; Chaves-Velasquez et al. (2017) figure 9, b4, figure 10, b2 and b3; GLA all orbits in figure 7; PKa especially figures 11 and 15; PWG figure 2, panels E and F; VSAD figure 4, 4th and 5th rows; WAM figure 5). Both  $x_{1v1}$  and  $x_{1v2}$  side-on profiles are the smoking gun of the existence of the  $vILR$  in the system, being introduced together at this resonance. Recently, Patsis & Harsoula (2018) have shown that it is the presence of the  $vILR$  that offers building blocks for the peanuts and as such can serve either regular or sticky chaotic orbits. Thus, the presence of the resonance is more important than the stability of the orbits. In PKa and in Patsis & Harsoula (2018) it is shown that the shapes of several 3D quasi-periodic orbits around  $x_1$ , have a morphology similar to that of the unstable one of the  $x_{1v1}$ ,  $x_{1v2}$  pair. Thus, in general, in the presence of a  $vILR$  resonance in a system, in order to find initial conditions of orbits that do not follow frown-smiles-like, or  $\infty$ -like trajectories in their side-on projections (at least during an important time interval), we have to avoid considering initial conditions in the regions of phase space, which are influenced by these three families. For this purpose, and as indicated by the figures in Katsanikas et al. 2013, PKa and Patsis & Harsoula (2018), we have to stay away from large volumes of phase-space around the main families of periodic orbits encountered beyond the  $vILR$  energy (in models that experience this resonance).

#### 6.4 Limits in the $\Delta E_J$ influence of a family, imposed by the evolution of its characteristic curve:

An ultimate limit of the extent of a family is put by its maximum  $E_J$  value beyond which the family does not exist. In such cases the characteristic of the family reaches a maximum  $E_J$  and then turns towards smaller  $E_J$  values. The most straightforward example one can bring is the  $x_1$  family itself in the case of type II gaps at the radial 4:1 resonance (Contopoulos 1988). In such a case, following the characteristic curve, we find that, as  $E_J$  increases, the  $x$  value first increases to reach a maximum  $x_0$  value and then decreases until a maximum  $E_J$  value. At this point it turns backwards towards smaller  $E_J$  values and towards the centre of the system (see e.g. figure 1 in Skokos et al. 2002a). Such regressions of the characteristic are especially important for the dynamics of slowly rotating bars (Skokos et al. 2002b; Tsigaridi & Patsis 2015). They are typical in the evolution of the families we presented in the tables. As an example we present in Fig. 8 the evolution of the stability indices of the  $vm33u$  family (red curves), after bifurcating from  $x_1$  considered 3-periodic (black curves). The morphology of this family is encountered in works by AVSD, PWG, VSAD and WAM. In this case  $E_{J_{max}} \approx -0.265$ . This evolution of the characteristic is com-

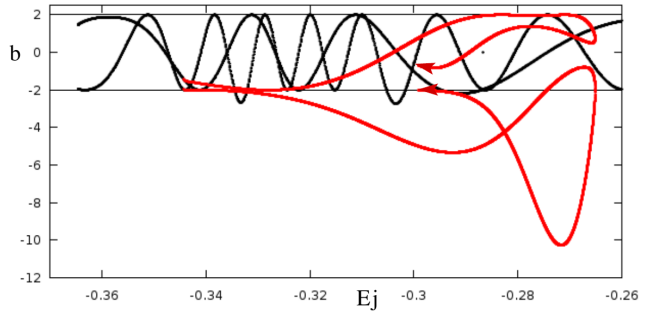


**Figure 8.** The evolution of the stability indices of the  $vm33u$  family (red curves), bifurcating from those of  $x_1$  at  $E_J \approx -0.344$ . After reaching a maximum  $E_J$  the  $vm33u$  family continues towards smaller energies.

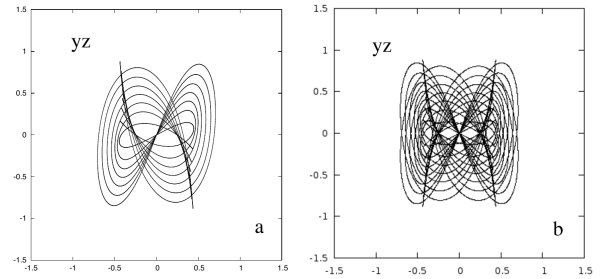


**Figure 9.** Seven  $vm33u$  periodic orbits at energies  $-0.34 \leq E_J \leq -0.28$ . In (a) we consider orbits belonging to one branch of the family, while in (b) we consider orbits from both branches symmetric with respect to the equatorial plane. In (b) we observe the appearance of two X features simultaneously.

mon among the  $mul$ -periodic orbits we found. One could conclude that the backwards evolving branch of the characteristic will bring more representatives of the family in the phase space at lower energies and thus its role in influencing larger areas of the phase space would be more important.

#### 6.5 Different families of p.o. offer different sizes of peanut building blocks.

In the case of the peanut structure, apart from the evolution of the characteristic of a family, there is also another property that has to be taken into account when its orbits are used as a building block for it. It is the length along the bar’s major axis within which this family can support the peanut and in general the size of the peanut it could support.

As we have seen in Patsis et al. (2002b) the morphological evolution of the orbits of the family reaches a  $y_{max}$  distance, beyond which the orbits grow practically only in the  $z$  direction. For building side-on profiles by using the orbits of the  $x_1$ -tree in 3D Ferrers bars this is an advantage, since it restricts the extent of the peanut to a fraction of the bar length of the order of half the distance to the end of the  $x_1$  bar, which is a desired property. For our model this does not hold in the case of the  $mul$ -periodic orbits that can be used as alternative solutions for the orbital content of the peanuts. We use again the orbits of the  $vm33u$  family to show this. In Fig. 9 we plot together the side-on projections of seven periodic orbits of the  $vm33u$  family at energies  $E_J = -0.34$  to  $-0.28$ , all of which are simple (vertical) unstable. In (a) we use orbits of one branch of the family, while in (b) we consider both its branches, symmetric to the

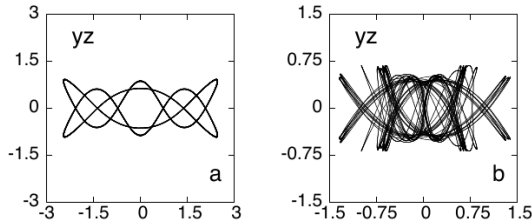


**Figure 10.** Structures that are formed in side-on projections, when we consider pairs of orbits, symmetric with respect to the equatorial plane. (a) The profile formed by the  $r_{\text{tv1}}$  family (Table 2). (b) A profile formed by a pair of symmetric, quasi-periodic orbits trapped around a stable representative of  $vm35u$  (Table 4).

equatorial plane. Ignoring the fact that these periodic orbits in our model are unstable, so that only sticky-chaotic orbits could possibly be used to populate a peanut structure, we observe that already at  $E_J = -0.28$ , the orbits contribute in growing a profile faster in the  $z$ - than in the  $y$ -direction. By including more orbits at larger energies, or orbits from the branch of the characteristic that goes backwards, towards the center of the system, we make the  $z_{\text{max}}/y_{\text{max}}$  ratio even larger as the projection of the orbits on the  $y$ -axis shrinks. We remind that the longest  $x1$ , bar supporting orbit reaches a 4.1 kpc distance along the major axis, and that the  $(E_J, y)$  coordinates of the  $L_1$  Lagrangian point are  $(-0.197, 6.2)$ . Thus, these orbits can support only features embedded in a boxy bulge in the central parts of the model. At any rate, the profile of the overlapping p.o. in (b) supports an overall boxy morphology, that harbours simultaneously two kinds of X-features; one with branches passing through the center of the system (“CX” in the terminology of Bureau et al. 2006) and another one with wings extending in a direction vertical to the  $y$ -axis (characterized as “OX” by Bureau et al. 2006). In galaxies, there are not known cases in which the two types of X coexist. Also the almost vertical orientation of the wings of the X is rather atypical. However, the stability and the extent of the  $vm33u$  family in our model does not allow us to investigate the dynamical mechanisms under which the appearance of just one of the X’s could prevail in profiles built by this family.

**6.6 The importance of combining symmetric branches of orbits and groups of orbits in a family for modelling morphological features:**

At a given energy, as we move from the centre of the main island of a simple-periodic orbit to its borders, we find in the surfaces of section groups of smaller and smaller islands. Since our model is 3D, these groups of islands are invariant tori belonging to the  $mul$ -periodic orbits described in our tables (see figures 14 to 17 in Katsanikas et al. 2011b). The existence of the  $mul$ -periodic orbits creates in phase space a zone of morphological influence, because these p.o. co-exist together with their symmetric, “twin”, orbits and their unstable counterparts. Symmetry, often helps in building orbital structures. Both “frowns” and “smiles” are needed to build the peanut by means of  $x1v1$  and  $x1v1'$  orbits. The plethora of orbits one can find in rotating triaxial systems offers a lot of examples of such pairs. In Fig. 10 we give two of them. In (a) we plot the side-on view of the  $r_{\text{tv1}}$  p.o. (see Table 2) together with its  $z$ -symmetric one, while in (b) we give a quasi-periodic orbit, together with its symmetric with respect to the equatorial plane, trapped around a stable representative of the  $vm35u$  family (Table 4) at  $E_J = -0.279$ ,

which has initial conditions  $(-0.0229, -0.4088, 0.2086, 0.0865)$ . The patterns formed in these profiles are promising for supporting an X feature. Nevertheless, in order to decide about the effectiveness of a family in building a structure, one needs to consider successive representatives of it and see if the feature to be modelled appears in such composite profiles. The most common example associated with the boxy bulges that describes the effect, is the way the frown-smile simple-periodic  $x1v1$  orbits support the X structure in them. It is not the wings of the frown-smile  $x1v1$  orbits that support it, but the fact that their apocenters are aligned along rays, which are eventually the branches of the X (see figure 19a in Patsis et al. 2002b, and especially figure 11 in PKa). The rays are a structure that appears in the composite profiles and not a morphological feature of the individual periodic orbits. Effects appearing in the orbital profiles after combining orbits from symmetric branches of a family, or after combining successive members of a family in an energy range, i.e. building composite profiles as in Patsis et al. (2002b), should be used as a criterion for qualifying or excluding this family from being considered as a building block for a specific morphological feature.

**6.7 Side-on and face-on boxiness:**

None of the *individual* face-on orbital patterns of the  $mul$ -periodic orbits is observed in real galaxies or in density maps of  $N$ -body simulations snapshots. For example, despite the fact that the  $rm21$  orbits are found in all models in the orbital studies we cite, their morphology does not appear in any galactic bar. However, when both  $y$ -symmetric orbits are taken into account a box is formed (Fig. 3). This is in agreement with the findings in PKb for the orbits in the  $vILR$  region that are responsible for the inner boxiness and with the conclusions of Chaves-Velasquez et al. (2017) for orbits encountered at all  $E_J$  along their characteristics. Boxiness in general is associated with quasi-periodic and sticky chaotic orbits close to the borders of the  $x1$  stability islands. This is exactly the region where we find  $mul$ -periodic orbits. We have to note that the possibility of the appearance of a morphological feature when sticky-chaotic orbits are integrated for long time cannot be a priori excluded. In PKb, in Tsigaridi & Patsis (2015) and in Chaves-Velasquez et al. (2017) such orbits are proposed for explaining the *face-on* X features that appears in some galactic bars. In the present paper this happens e.g. with the orbits in Fig. A1b,c (considering also their  $y$ -symmetric counterparts) if integrated for long enough. However, since we did not find another similar case, based on families with  $n \geq 2$ , in order to decide about the generality of this dynamical mechanism, a model-dependent systematic study is needed.

For the edge-on profiles, We observe that the larger the multiplicity, the more boxy the side-on view of the family is. The same holds for the  $E_J$  at which a family is introduced in the system for all families of a certain multiplicity. The larger the  $E_J$  at which it is bifurcated from  $x1$  the  $mul$ -periodic family, the more boxy is its side-on view. This is the reason why we stopped giving the profiles of more orbits bifurcated from  $x1$ , as the stability curves of this family vary (Fig. 2 and Fig. 4). In general, for p.o. of high multiplicity, and for those bifurcated at large  $E_J$ , morphologies can be simply characterized as complicated Lissajous patterns and an overall boxiness is the only feature of their morphology.

### 6.8 The complexity of the structure of phase space increases as we approach corotation:

The morphology of an orbit at a given energy depends on the families of resonant periodic orbits that exist at that energy, on their stability that will determine the phase space structure at their neighbourhood (see Katsanikas & Patsis 2011; Katsanikas et al. 2011, 2013), as well as on the location of the initial conditions of the orbit in phase space. With increasing energy, i.e. moving from the center towards corotation, we reach progressively more radial and vertical resonances, so new families are introduced in the system and thus the structure of phase space becomes more complex. Orbits with initial conditions that are close to each other will probably follow totally different trajectories. This is an expression of the presence of chaos close to corotation, as in 2D systems (Contopoulos 1981). This hinders the growing of structures like bars at this region.

### 6.9 The *mul*-periodic orbits are more important at the central parts of the bars.

The *mul*-periodic orbits we consider as building blocks of the orbital patterns encountered in the papers we cite, are bifurcated at low energies. Thus they are important for the inner morphology of the bars, at distances from the center up to half the length of the semimajor axis. Most orbits given in our Tables have sizes that in our model would contribute only in the central parts of the bars. For example, orbits with simple shapes like those of the *vm31* family<sup>4</sup>, if populated, would be found, in most models, embedded in the central parts of the galaxies, not being able to affect the overall morphology of a bar, neither face- nor edge-on. This is probably the reason that this family is not traced in other papers, despite its promising shape, especially if both  $z$ -symmetric branches are considered.

### 6.10 *mul*-periodic bifurcations at high energies:

We find that *mul*-periodic bifurcations of *x1* and *x1*-tree families at high energies, as well as the planar families beyond the 4:1 resonance gap and its bifurcations at those energies, are in general not bar-supporting. They correspond to regions of the bar beyond its inner thick part, or beyond the end of the bar altogether. Their morphological evolution as  $E_J$  increases is towards rounder shapes than the elliptical projections of the *x1*-tree orbits on the equatorial plane.

As a further, albeit less strong, obstacle for higher multiplicity p.o. to determine morphological profiles, is that higher multiplicity families have longer periods and thus would need longer times to impose their individual morphologies in all three projections. Indeed, one can intuitively understand this by considering that exactly at the bifurcating point the representatives of the mother and child families are morphologically identical, while the period of the “mother” is  $T$  and the period of the “child” is  $mulT$ . As  $E_J$  increases both  $T$  and  $mulT$  increase. As an example we give in Table 6 the periods of *x1* and *rm21* p.o. in the interval  $-0.331 < E_J < -0.312$ , in which *rm21* exists in our model. Despite

<sup>4</sup> The edge-on views of this family resemble a shape encountered already in orbits found in triaxial systems, called “pretzel” by Merritt & Valluri (1999, see their figure 4). We do not give to it any name here, to avoid confusion, since a similar term is used by PWG for the side-on shape we find in our *vm33u* orbits.

**Table 6.** The periods of *x1* and *rm21* families in the interval  $-0.331 < E_J < -0.312$ . We have always  $T(x1) < T(rm21)$ .

| $E_J$     | -0.331 | -0.33 | -0.325 | -0.32 | -0.315 | -0.312 |
|-----------|--------|-------|--------|-------|--------|--------|
| $T(x1)$   | 23.1   | 23.8  | 26.8   | 29.8  | 32.7   | 34.5   |
| $T(rm21)$ | 46.2   | 46.8  | 49.3   | 51.5  | 53.5   | 54.3   |

the fact that the  $T(rm21)/T(x1)$  ratio decreases with the energy, it is always larger than one.

### 6.11 Model-dependency of the orbits and their role for supporting specific structures:

The orbits we are presenting are not a special class of orbits existing in our specific model or in rotating Ferrers bars. The orbits, each one with its own characteristic morphology, are linked to the radial and vertical resonances of any rotating, triaxial potential in autonomous Hamiltonian systems. Thus, the patterns we observe in the Tables of this paper, as well as those of the 1-periodic orbits in Skokos et al. (2002a), have been encountered in several different models that may include a Ferrers bar or not. Thus, they are expected to exist also in models with a peanut-shaped bar. In this case their relative importance for reproducing a peanut morphology should be estimated by means of Schwarzschild-type, self-consistent models. Alternatively, one can use an  $N$ -body snapshot from which we can obtain the potential and forces, as well as all the individual orbits that constitute it. We will follow this latter alternative in future papers.

### 6.12 The role of chaotic orbits:

We note that in many cases of orbits, the morphological patterns encountered in orbital analyses correspond to families that are mainly *unstable*. This can happen either because these families are unstable over large  $\Delta E_J$  intervals, or even because they are introduced as unstable and remain unstable as  $E_J$  varies. (see e.g. the example described by Patsis & Harsoula 2018). If such families prevail in realistic models indeed, then either the role of sticky chaotic orbits in building the bars (PKa,b) is much more pronounced than appreciated until now, or we have mass distributions, where the stability of the main families is different than in the known, analytic models.

The main point of the present paper was to indicate the origin of *mul*-periodic orbits and discuss the obstacles they have to overcome in order to become important for the overall morphology of galactic bars. We also compared their morphology with orbital patterns found and presented in several relevant works. In the subsequent papers of this series, we will investigate the relative contribution of the orbits presented here in shaping the morphology of specific 3D  $N$ -body bars.

### Acknowledgements

We thank Prof. G. Contopoulos for fruitful discussions and very useful comments. This work has been partially supported by the Research Committee of the Academy of Athens through the project 200/895. PAP thanks the financial support of Aix Marseille Université for a 2-month visiting professorship at LAM.



## REFERENCES

- Abbott C. G., Valluri M., Shen J., Debattista V. P., MNRAS 470, 1526 (AVSD)
- Athanassoula E., 1992, MNRAS 259, 328
- Athanassoula E., 2016, in *Astrophysics and Space Science Library* 418, Galactic Bulges, E. Laurikainen, R. Peletier, D. Gadotti (eds.), Springer International Publishing, Switzerland, p. 391
- Athanassoula E., Beaton R. 2006, MNRAS, 370, 1499
- Athanassoula E., Bienayme O., Martinet L., Pfenniger D. 1983, A&A 127, 349
- Athanassoula E., Laurikainen E., Salo H., Bosma A. 2015, MNRAS, 454, 3843
- Athanassoula E., Romero-Gómez M., Bosma A., Masdemont J. 2010, MNRAS, 407, 1433
- Broucke R., 1969, NASA Techn. Rep. 32, 1360 609
- Bureau M., Aronica G., Athanassoula E., Dettmar R.-J., Bosma A., Freeman K. C., 2006, MNRAS, 370, 753
- Chaves-Velasquez L., Patsis P. A., Puerari I., Skokos C., Manos T. 2017, ApJ 850, 145
- Chaves-Velasquez L., Patsis P. A., Puerari I., Moreno E., Pichardo B., 2019, ApJ in press (arXiv:1812.04068)
- Contopoulos G., 1981, A&A 102, 265
- Contopoulos G., 1983, ApJ 275, 511
- Contopoulos G., 1986, Celest. Mech. 38, 1
- Contopoulos G., 1988, A&A 201, 44
- Contopoulos G., 2004, "Order and Chaos in Dynamical Astronomy", Springer-Verlag, Berlin, Heidelberg, New York
- Contopoulos G. & Grosbøl P., 1989, A&ARv, 1, 261
- Contopoulos G. & Harsoula M., 2008, Int. J. Bifurc. Ch. 18, 2929
- Contopoulos G., Magnenat P., 1985, Celest. Mech. 37, 387
- Contopoulos G. & Papayannopoulos T., 1980, A&A 92, 33
- Deibel A.T., Valluri M., Merritt D., 2011, ApJ 728, 128 Elmegreen
- Erwin P., Debattista V. P., 2013, MNRAS, 431, 3060
- Ferrers, N. M. 1877, Quart.J.Pur.Appl.Math., 14, 1
- Gajda G., Łokas E. L., Athanassoula E. 2016, ApJ 830, 108 (GLA)
- Hadjidemetriou J., 1975, Celest. Mech., 12, 255
- Katsanikas M., Patsis P.A., 2011, Int. J. Bif. Ch. 21-02, 467
- Katsanikas M., Patsis P.A., Pinotsis A.D., 2011b, Int. J. Bif. Ch. 21-08, 2331 (KPP)
- Katsanikas M., Patsis P.A., Contopoulos G., 2011, Int. J. Bif. Ch. 21, 2321
- Katsanikas M., Patsis P.A., Contopoulos G., 2013, Int. J. Bif. Ch. 23-02, 1330005
- Machado R.E.G., Manos T., 2016, MNRAS 458, 3578
- Manos T., Athanassoula E., 2011, MNRAS 415, 629 M., Merritt D., Valluri M., 1999, AJ 118, 1177
- Miyamoto M., Nagai R., 1975, PASJ 27, 533 Springer
- Patsis P. A., Zachilas L., 1990 A&A 227, 37
- Patsis P. A., Grosbøl P., 1996, A&A, 315, 371
- Patsis P. A., Athanassoula E., Quillen A. C., 1997, ApJ, 483, 731
- Patsis P. A., Athanassoula E., Grosbøl P., Skokos Ch., 2002, MNRAS 335, 1049
- Patsis P. A., Skokos Ch., Athanassoula E., 2002, MNRAS 337, 578
- Patsis P. A., Harsoula M., 2018, A&A 612, 114
- Patsis P. A., Kalapotharakos C., Grosbøl P., 2010, MNRAS 408, 22
- Patsis P. A., Katsanikas M., 2014, MNRAS 445, 3525 (PKa)
- Patsis P. A., Katsanikas M., 2014, MNRAS 445, 3546 (PKb)
- Patsis P.A., Zachilas L., 1994, Int. J. Bif. Ch. 4, 1399
- Pfenniger D., 1984, A&A 134, 373
- Plummer H.C., 1911, MNRAS 71, 460
- Poincaré H., 1899, Les Methodes Nouvelles de la Mechanique Celeste, Vol. III, Gauthier-Villars, Paris
- Portail, M., Wegg C., Gerhard O., 2015, MNRAS 450L, 66 (PWG)
- Heisler J., Merritt D., Schwarzschild M., 1982, ApJ 258, 490
- Skokos Ch., Patsis P. A., Athanassoula E., 2002a, MNRAS 333, 847
- Skokos Ch., Patsis P. A., Athanassoula E., 2002b, MNRAS 333, 861
- Tsigaridi L., Patsis P.A., 2015, MNRAS, 448, 3081
- Valluri M., Shen J., Abbott C. G., Debattista V. P., ApJ 818, 141 (VSAD)
- Wang Y., Athanassoula E., Mao S., 2016, MNRAS 363, 3499 (WAM)
- Wozniak H., Michel-Dansac L., 2009. A&A 494, 11 (WM-D)

## APPENDIX A: QUASI- AND NON-PERIODIC ORBITS

In Sections 3 and 4 we have indicated the origin of the main 2-, 3-, 4-, 5- and 6-periodic bifurcations of the planar x1 family, while in Section 5 we examined the role of *mul*-periodic orbits with large energies in determining the structure of the bar. The structure of these orbits has to be compared with the morphology of orbits encountered in the relevant literature, which are clearly not periodic (or at least not *mul*-periodic with a small *mul*). The peanut-supporting orbits depicted in the papers we mentioned in the introduction, point either to quasi-periodic, or to sticky-chaotic orbits behaving like regular for a reasonably long time.

Periodic orbits are mathematical objects and can be considered as the backbone of the phase space in a system. However, in order to follow orbits that are more frequently found in realistic barred galaxy potentials, those of real galaxies, or of simulated ones, one has to integrate initial conditions away from those that exactly correspond to a periodic one. The periodic orbits structure the phase space and their presence influences the morphology of other quasi- or non-periodic orbits at the same energy. In 2D models for galactic bars we have described this already in Patsis et al. (1997) for orbits that support the outer boxiness of the bars. The orbital patterns we had found in that paper were hybrid morphologies of existing periodic orbits, which can be stable or unstable.

One can get a fair impression of the possible morphologies that can be supported at a given energy by simply integrating directly a number of initial conditions on a dense grid imposed on a 2D surface of section. This gave useful results in a number of studies (see e.g. Patsis et al. 2010; Tsigaridi & Patsis 2015). Unfortunately, and contrary to 2D models, in 3D systems, starting perturbing planar orbits for example in  $(x, p_x)$  surfaces of section, can only reveal a subset of the morphologies that can be encountered. The Poincaré surfaces of section are 4D and so, the initial conditions of a single p.o. are subject to perturbations in four directions. Constructing a dense 4D grid will lead to a huge amount of data and this is not easily manageable.

The information we get by inspecting a 2D surface of section in a 2D model is not available in the 4D surfaces of section in 3D autonomous Hamiltonian systems. It is not only that we cannot directly classify as regular or chaotic an orbit by simple inspection of the location of its initial condition on the surface of section, but it is mainly the inability to trace the relative location of the stability

islands around a stable p.o. in the chaotic seas, in which they are embedded. Thus, it is difficult to delimit zones of morphological influence of a p.o. in phase space. Although we could visualize 4D invariant tori of stable p.o. (Patsis & Zachilas 1994; Katsanikas & Patsis 2011) and in some cases the manifolds associated with unstable p.o. (Katsanikas et al. 2011, 2013) in the 4D spaces of section, we could only in few specific cases navigate ourselves in regions of the 4D space, where several islands of periodic orbits co-exist (Katsanikas et al. 2013, PKa, KPP). Nevertheless, in the present study we disturbed a large number of characteristic planar and 3D *mul*-periodic orbits and we succeeded in finding quasi- and non-periodic orbits with morphologies pointing to structures that could be related to the peanut or X-shaped structures (e.g. frown-smile shapes), which we encounter in 3D bars.

Even though perturbing p.o. in a non-systematic way does not provide all the information that a systematic search would, it can still be most useful. The first thing that one can estimate is the easiness or difficulty with which some patterns appear in the three projections of orbits in different models. As expected, the patterns that one encounters easier are associated with the presence of 1-periodic orbits, since the latter are found in the centres of stability islands that occupy large volumes in the phase space. In barred galaxy models these orbits are the *x1* family and its 1-periodic 3D bifurcations that build the *x1*-tree (Skokos et al. 2002a), which have elliptical shapes in the  $(x, y)$  plane. Three-dimensional, non-periodic orbits with elliptical projections on the equatorial plane can be found either by perturbing quasi-periodic orbits corresponding to invariant curves *close to* *x1* in  $(x, p_x)$  surface of section, or by perturbing one or more of the four initial conditions of the 3D orbits belonging to the families of the *x1* tree (*x1v1*, *x1v2* etc.). Independently of their origin and their regular or sticky-chaotic character, the supported elliptical morphologies on the equatorial plane are almost identical and are ubiquitous in papers about orbits in barred galaxy models (e.g. the orbits in figure 6, 3rd row in AVSD; the orbits in figure 3, 1st row and the orbits in figure 10 in Chaves-Velasquez et al. (2017); the orbits in figures 6, 1st row and figure 7, 1st and 2nd rows, in GLA; the orbits in figures 3 and 4 in KPP; the orbit in figure 15 in PKa; the orbits in figure 1, three first rows, in figure 3, 1st row, right, and figure 4, 4th and 5th row in VSAD; the orbits in figures 10 and 11 in WM-D etc.). In order to avoid elliptical shapes in the  $(x, y)$  projections of the orbits, one has to deviate more from the initial conditions of the *x1* or *x1*-tree orbits and consider orbits close to the edges of the stability islands (both at their “regular” and their “chaotic” side). This can lead to single (only in one projection), or double (both in their face-on and edge-on views) boxiness of orbits of galactic bars (Chaves-Velasquez et al. 2017) and can be particularly important for the structure of the peanuts when we consider orbits in the *vILR* resonance region (PKb).

Depending on the various resonant families that exist at a given energy, the face-on view of a quasi- or non-periodic orbit can be combined with different side-on projections. We give as an example three 3D orbits with face-on views pointing directly to the planar *rm21* family (Fig. A1). As we already commented, the frequency with which the *rm21* morphology appears in orbits presented in the orbital studies of rotating barred potentials is large (see section 2.2 above). This is due to the fact that it exists in considerable energy ranges in the models, close to the *vILR* region, and its stability islands, together with those of *rm22*, always surround the very central invariant curves around *x1*, forming a zone of morphological influence in this area (see e.g. Fig. 1). By inspecting of surfaces of section like the one in Fig. 1, we realize e.g. that orbits with a  $|\Delta p_x| \gtrsim 0.1$  from the periodic orbit, enter the zone of

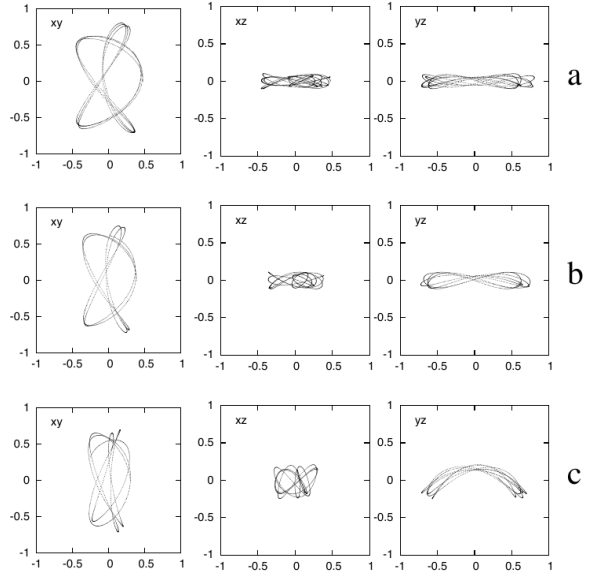


**Figure A1.** Three 3D orbits that have in their face-on projection an *rm21*-like morphology. This is combined in (a) with a boxy side-on view, in (b) with a *x1v2*-like, and in (c) with a *x1v1*-like one.

influence of the *rm21* and *rm22* families. This can easily happen if the dispersion of velocity is locally slightly increased in a model. In other cases of stronger bars, there is also a sticky zone with orbits of similar to *rm21*, *rm22* and *rm21u*, *rm22u* morphologies around the *x1* stability island (a characteristic case is given in figure 1 in PKb).

By perturbing these regular and/or sticky chaotic orbits in the vertical direction we reach orbits that retain until a certain value of the perturbation the *rm21* face-on morphology. However, they differ between them in their edge-on projections. The latter depend on the location of the  $z, p_z$  initial conditions in the 4D space of section, which we use. It is difficult to predict a priori how the morphology of quasi-periodic orbits, or of orbits on manifolds, changes as we move along a certain direction in phase space. Until now it has been described only in particular cases, such as the case of the *x1*, *x1v1* and *x1v2* orbits in Katsanikas et al. (2013) and in PKb. In general we could say that the morphology is influenced by the proximity of the initial conditions of an orbit to those of other periodic orbits at the same energy. The orbits in Fig. A1 are integrated for a few *rm21* periods and have in (a)  $E_j = -0.32396$  with initial conditions  $(0.475, 0, 0, 0.05)$ , in (b)  $E_j = -0.3268$  and  $(0.385, 0.06, 0, 0)$  and in (c)  $E_j = -0.3268$  and  $(0.3, 0.14, -0.02, 0.03)$ . We can clearly see the similarity of their  $(x, y)$  projections with the orbits of the *rm21* family, while the side-on views are different. The side-on view of the orbit in Fig. A1a can be characterized just “boxy” already just after three *rm21* orbital periods, while those of Fig. A1b and Fig. A1c are similar for example with those in figure 7, 4th row and figure 7, 3rd row in GLA, respectively. They have a *x1v2*-like (Fig. A1b) and a *x1v1*-like (Fig. A1c) side-on morphology. Also in WAM (figure 5, 2nd and 3rd column) we encounter orbits with similar combinations of face- and side-on profiles as in Fig. A1b and c. We can find more edge-on profiles combined with *rm21* face-on morphologies, if we consider also quasi- and non-periodic orbits associated with its 3D bifurcations, as e.g. the *rm21\_vm4* orbit given in Table 2 or the orbit in figure 2 in Katsanikas et al. (2011b).

In reverse, basing ourselves on the edge-on views, at energies

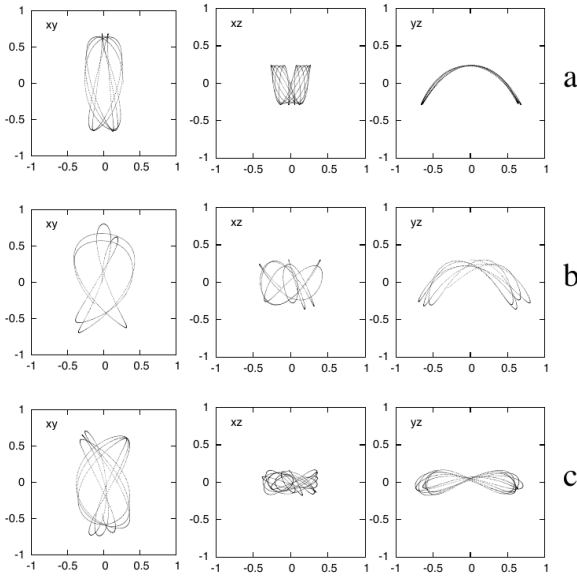


**Figure A2.** Face-on rm21u and rm22u morphologies combined with side-on  $x1v1$ -like (a) and (b), and  $x1v2$ -like shapes (c).

larger than those of the vILR region, the 3D orbits that have side-on profiles pointing to the  $x1v1$  and  $x1v2$  families are ubiquitous. Besides the quasi-periodic orbits of these two families (with elliptical or boxy face-on projections) and their associated sticky orbits, frown - smiles and “ $\infty$ ”-like edge-on profiles can be found combined with various face-on morphologies. The morphology of the planar unstable families rm21u and rm222u, bifurcated together with rm21 and rm22, can also support the known profiles of the vertical families bifurcated at the vILR. Examples are given in Fig. A2. In (a) we have an orbit with an rm21u-like face-on morphology with  $E_J = -0.32281$ , and initial conditions  $(0.266, 0.24, 0, 0)$ , in (b) a rm21u-like orbit with  $-0.318$ ,  $(-0.026, 0.3, 0, 0)$  and in (c) a rm22u-like orbit with  $-0.3268$ ,  $(0.168, 0.07, 0.12, 0)$  respectively (the rm21u and rm22u families have the same morphology, and symmetric with respect to the  $x$ -axis). The combination of face-on and side-on views of the orbit in Fig. A2b is encountered also in figure 7, 5th row in GLA, while different side-on views in combination with an rm21u-like face-on morphology are found in orbits mentioned at the last column of the rm21u entry in Table 2. The rm21u and rm22u are the unstable p.o. we find between the rm21 and rm22 stability islands (Fig. 1). Thus, their morphology is also a common one.

Besides the  $x1v1$  and  $x1v2$  edge-on profiles, the next common morphology that is encountered in the various models, is a boxy one, with sharply defined edges, but without a particular morphology inside the box. The mechanism that favours the appearance of such a structure, instead of a particular edge-on shape, is presented in PKb and in Chaves-Velasquez et al. (2017). Apart from the cases that are presented in these two papers, many examples of boxy orbits can be found in the relevant literature, as e.g. in AVSD (figure 6, 1st and 4th row), Deibel et al. (2011) (figure 11), GLA (figure 6, two last rows), VSAD (all orbits in figure 1 and the orbits in figure 4, three first rows), WAM (figure 21, first and last columns).

Coming to discuss the side-on profiles in Fig. A3, we need to specifically mention the side-on profiles given in figure 2 in PWG. While the orbits in panels E and F of their figure 2 point to sticky chaotic and quasi-periodic,  $x1v1$ -like morphologies re-

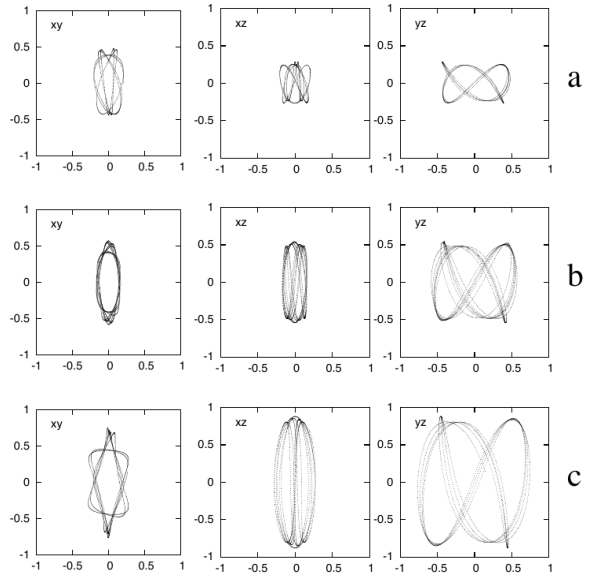


**Figure A3.** Three profiles of 3D orbits with vm33u-like side-on views, but with considerably different face-on views. The energies of the orbits increase from  $-0.333$  (a), to  $-0.31$  (b), and to  $= -0.28$  (c). We observe that the  $z_{max}/y_{max}$  ratio increase with the energy.

spectively (with any kind of face-on projection they may be combined), those in panels A to D are almost absent from the rest of the orbital studies we cite. An exception is the profile in panel C, emphasized in their figure 5 bottom, which appears also in figure 6, last row in AVSD, in figure 4, last row in VSAD and in figure 21 (2nd and 3rd columns) in WAM. The side-on morphology of all these orbits points directly to vm33u, the unstable, 3-periodic vertical bifurcation of  $x1$  at its second tangency with the  $b = -2$  axis, when it is also considered to be 3-periodic (see Table 4). Three non-periodic orbits that retain the side-on vm33u morphology are given in Fig. A3. The orbits are vertically unstable (the vertical index  $b2 = -5.3$  at  $E_J \approx -0.29$ ), so the depicted side-on structure is preserved only when small radial deviations from the initial conditions of the p.o. are applied. In Fig. A3a we have  $E_J = -0.333$  and  $(0.2, 0.203, 0.02, -0.082)$ . In Fig. A3b we have respectively  $-0.31$  and  $(0.15, 0.398, 0.0182, -0.137)$ , which are the initial conditions of the periodic orbit at the same energy, differing only by  $\Delta x_0 = 0.0074$ . The orbit is integrated for about three orbital periods of the periodic orbit. By continuing the integration for two more periods, the morphology becomes boxy. In Fig. A3c,  $E_J = -0.28$  and the initial conditions  $(0.190, 0.695, 0.0486, -0.1396)$ . In this case we observe, that the  $z$ -dimension of the orbit is larger than the one along  $y$ . The fact that the side-on views of the orbits reach a maximum length (i.e. a maximum extent along the  $y$  axis) at a given energy, beyond which they practically increase only in height, is a known property of the 3D orbits in Ferrers bars. It has been discussed in Patsis et al. (2002b) in relation to the extent of the  $x1v1$  peanut and we will also return to this in Section 6. The family becomes stable in our model at even larger energies, where the  $z_{max}/y_{max}$  ratio of the orbits is even larger. The face-on view of the orbit combined with the vm33u profile given by PWG in their figure 5, top, belongs to the rm21-like patterns, with an asymmetry in its loops that is typical for many of the orbits we encountered. We give in Fig. A4 an example of an orbit with  $E_J = -0.3268$ ,  $(0.138, 0.05, 0.12, 0)$ , for which we take initial condi-

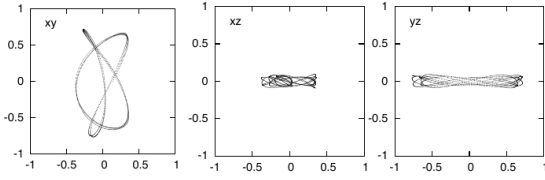


**Figure A4.** An orbit with initial conditions on an rm21 stability island perturbed in the vertical direction, at  $E_J = -0.3268$ .

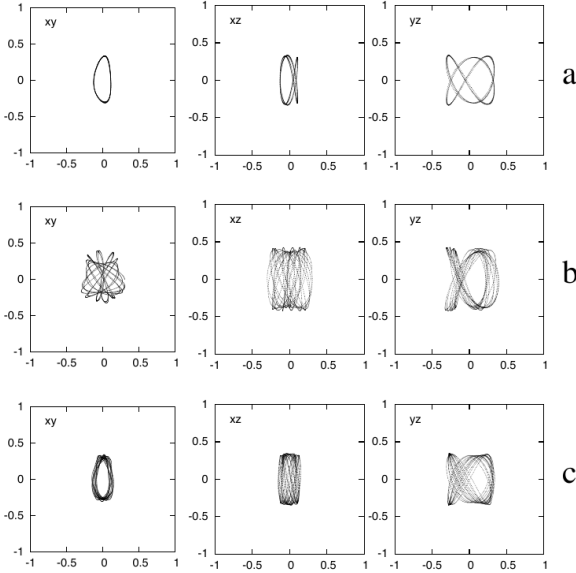


**Figure A5.** Three examples of 3D orbits reproducing the side-on profile of the unstable family  $x1mul2u$  ( $vm21u$ ). In (a) and (c) they are for energies  $-0.333$  and  $-0.33307$ , while in (b) for  $-0.325$ .

tions on a stability island in the  $(x, px)$  plane of section belonging to rm21 and we add  $z = 0.05$  in its initial conditions. So, here we have one more example of different morphological combinations in different projections.

We find similar results for the profile in panel A in figure 2 in PWG. It is the family bifurcated from  $x1$ , at the same energy as  $x1mul2$ , but as unstable. Despite the fact that we did not encounter a similar side-on profile in other studies, we note that it is easily obtained by perturbing orbits of the stable family ( $x1mul2$ ), underlying the fact that the initial conditions of the representatives of the two families at a given energy are close. In Fig. A5 we give three such characteristic orbits. In (a) we have an orbit with  $E_J = -0.333$  and initial conditions  $(0.108, 0.294, -0.0066, 0.0537)$ , in (b)  $-0.325$  and  $(0.3, 0.13, -0.007, 0.2)$ , while in (c)  $-0.33307$  and  $(0.08, 0.3, 0, -0.05)$  respectively. Here we have a situation similar to the one presented by Patsis & Harsoula (2018) for the  $x1v1/x1v2$  pair, where at a given energy side-on profiles can be easily built either by quasi-periodic or by sticky chaotic orbits.

Finally, we note that there is a class of non-periodic orbits, well represented in papers with orbital studies, with a characteristic shape in their face-on views. Most of them have morphologies similar to rm21u at energies much larger than the one at which this family introduced in the system. Two examples are given in Fig. A6. The orbit in (a) has  $E_J = -0.319$  and initial

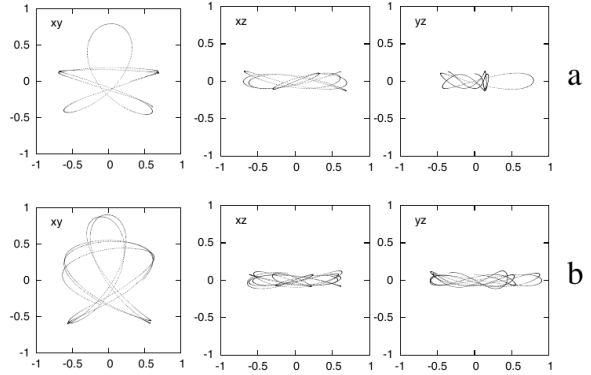


**Figure A6.** Two examples of 3D orbits with similar lengths along the  $x$  and  $y$  axes. They are typical in bar orbital studies and may contribute in building the bar central parts.

conditions  $(0.306, 0.1, 0.23, 0)$ , while the one in (b)  $-0.318$  and  $(0.47, 0.07, 0.13, 0)$  respectively. Their face-on structure is similar to the one of orbits like the one in figure 11, middle row in Deibel et al. (2011), the orbit in figure 3, 3rd row right, in VSAD or the orbit in figure 5, left column, in WAM. These orbits reflect the morphological evolution of the rm21 and rm22 pair of families as energy increases. Such orbits, not being elongated along the major axis of the bar can populate only the central parts of galactic bars, and can be associated with the thick part of the bar.